Signatures of temporary charge carrier trapping

by single quantum dot spectroscopy and spectroelectrochemistry

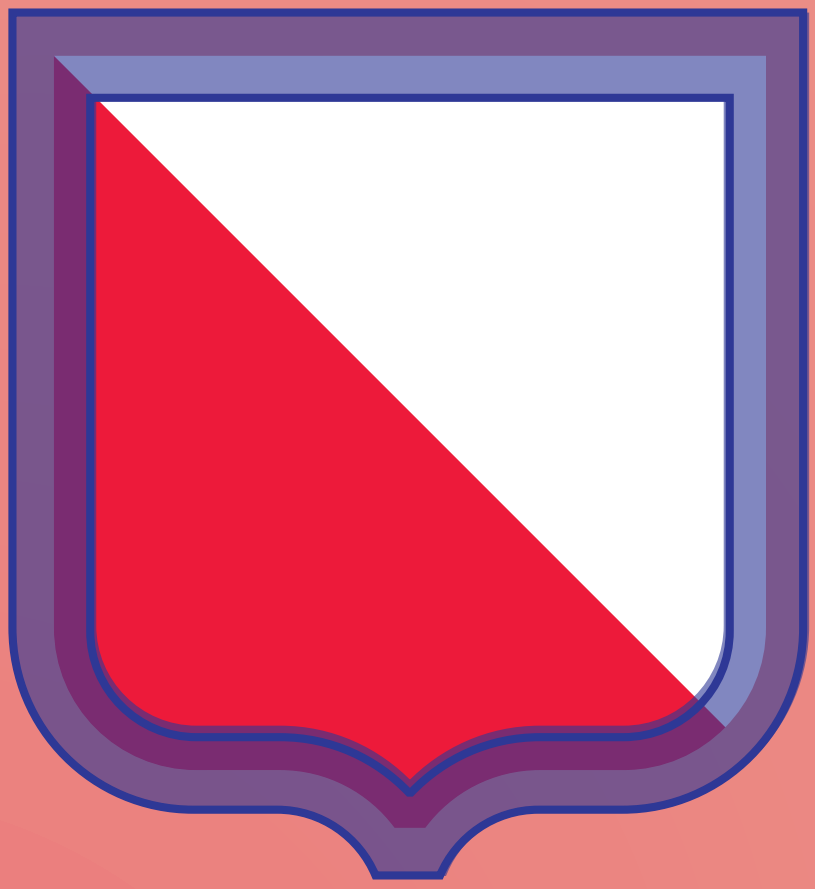

Sander Vonk

First name: Sander Jan Wilhelmus
Last name: Vonk
Student number: 3974073
Contract period: February 5, 2018 – March 30, 2019
Daily supervisor: Stijn O.M. Hinterding, Msc
Supervisor: Dr. Freddy T. Rabouw
Second supervisor: Prof. Dr. Alfons van Blaaderen

Contents

Chapter 1

Introduction

Over 30 years ago, Murray et al. first reported a successful synthesis method to make highly monodisperse fluorescent colloidal quantum dots (QDs).[1] From that moment on, colloidal QD research flourished, aiming at optimizing and understanding the optical properties. Because of their high versatility in size, shape and luminescent properties, colloidal QDs found their way to industry in many applications like single-photon emitters, photocatalysis and biomedical imaging.[2, 3, 4, 5]

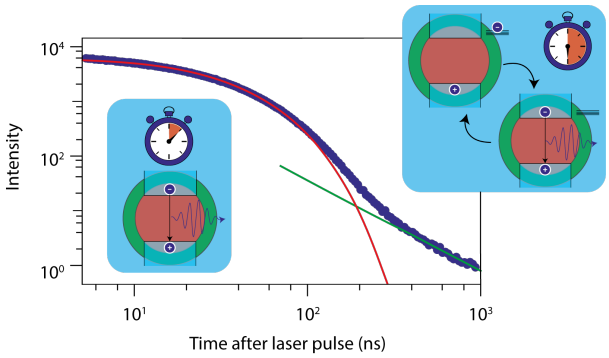

Figure 1.1: Prompt emission and delayed emission of a single colloidal quantum dot. Direct recombination of an excited quantum dot results in photon emission, typically 100 ns after excitation. Sometimes emission takes significantly longer, 100 ns – several μs , caused by temporary trapping of a charge carrier. This phenomenon is called delayed emission.

In 1996, QD research received another boost by the first reported research on single QDs by Nirmal et al.[6] They showed that fluorescence of QDs is not constant in time but random blinking events between a bright and a dim state occur. Since blinking is unwanted for many applications, various theoretical and experimental work since then aimed on on elucidating the microscopic origin of this peculiar phenomenon.[7, 8, 9]

Recent experimental evidence shows that blinking might be closely related to a phenomenon called delayed exciton emission.[10, 11] Trapping and subsequent release of excited charge carriers results in photon emission relatively long after excitation. Usually delayed exciton emission is overlooked due to the relatively low intensity (see figure 1.1 (**a**)). While the intensity of delayed emission is rather low, the total fraction of photons arising from delayed emission can be around 15 – 50 %.

In this thesis we will contribute to the fundamental understanding of charge carrier trapping in core/shell QD systems, hopefully paving the way to a more microscopic understanding of the phenomenon which ultimately might lead to full control over blinking.

Outline of this thesis:

Chapter 2 – provides a theoretical background on topics relevant for the rest of the thesis. First an introduction is given on excitation of semiconductor nanocrystals and possible decay paths to the ground state. Lastly, an elaborate discussion of existing delayed emission models is given and possible explanation of its origin.

Chapter 3 – provides an overview of the experimental methods used in this research.

Chapter 4 – shows experimental results on the prompt and delayed emission of excitons in CdSe/CdS core/shell QDs. First an elaborate experimental overview is given of two main blinking models commonly observed in colloidal QDs. Knowledge about these blinking processes will be exploited in the second half of this chapter to understand delayed emission on a single QD scale. Two different mechanisms contributing to delayed emission will be introduced and thoroughly characterised.

Chapter 5 – shows experimental results on the prompt and delayed emission of excitons in CdSe/CdS/ZnS QD films as a function applied voltage. We will model changes of prompt emission as function of applied voltage by introducing a Fermi-Dirac model which explains the gradual shift from neutral to charged and eventually doubly charged QDs. In the second part of this chapter we use these results to explain quenching of delayed emission as a function of voltage and give an elaborate discussion about the implications.

Chapter 6 – provides a small overview of the obtained results and contains suggestions for future research.

Chapter 2

Theoretical background

Abstract **– This chapter introduces the fundamentals of quantum dot emission and absorption. We will explain the decay dynamics of direct recombination of an exciton. Next, the influence of additional charge carriers in the emissive state will be discussed. Finally, an elaborate overview of existing delayed emission models and possible chemical origins of trap states contributing to this peculiar phenomenon is given.**

2.1 Colloidal quantum dots

In 1993, Murray et al. first reported on the synthesis of highly monodisperse Cd-based quantum dots (QDs).[1] They showed that hot injection of precursors results in a nearly perfectly mono-disperse QD dispersion. The controlled fabrication of such small crystals can be explained by classical nucleation theory. In only a small amount of time (e.g. just after injection of the precursor) all crystal nuclei are formed. After nuclei formation, slow growth at lower temperatures ensures gradual growth of all crystals in solution. By changing the length of the growth period one can change the size of the QDs. Interestingly, by controlling the size of the QDs the photoluminescence (PL) properties change considerably.[12]
To understand this, let us first consider two atoms forming a chemical bond in figure 1.1 (**a**). We know that, upon formation of this bond, the two atomic orbitals overlap and form an anti-bonding and a bonding molecular orbital which are separated by a certain energy. For a semiconductor, if we consider many of these atoms in a crystal the orbitals form a continuous band of energy levels called the valence band. This band is completely filled with electrons and contributes to chemical bonding in the crystal. Separated by an energy difference, e.g. the bandgap, the orbitals also form a continous band called the conduction band. The conduction band is anti-bonding. Colloidal QDs fall somewhere in between these two extremes where the radius is only 2 – 10 nm. Because the energy difference between the conduction and the valence band typically lies between 1.9 – 2.5 eV, visible or UV light can be used to promote an electron from the valence band to the conduction band as can be seen schematically in figure 1.1 (**b**). Figure 1.1 (**c**) shows the absorption spectrum of a CdSe core-only sample in blue. The excited electron will form a bound state with the hole left in the valence band. After some time the electron will recombine with the hole again, emitting light precisely matching the energy of the

bandgap. This bound state is called an exciton and is delocalized throughout the QD crystal.[13] An exciton in bulk CdSe has a characteristic radius of 5.6 nm called the excitonic Bohr radius.[14] Comparable size of the QDs and the excitonic Bohr radius gives rise to an effect called quantum confinement. The wavefunction is more confined if the crystal gets smaller thereby increasing the bandgap. In this way, the emission colour of QDs can be tuned by simply changing the size as can be seen in the colour rainbow formed by differently sized CdSe QDs in figure 1.1 (**d**).

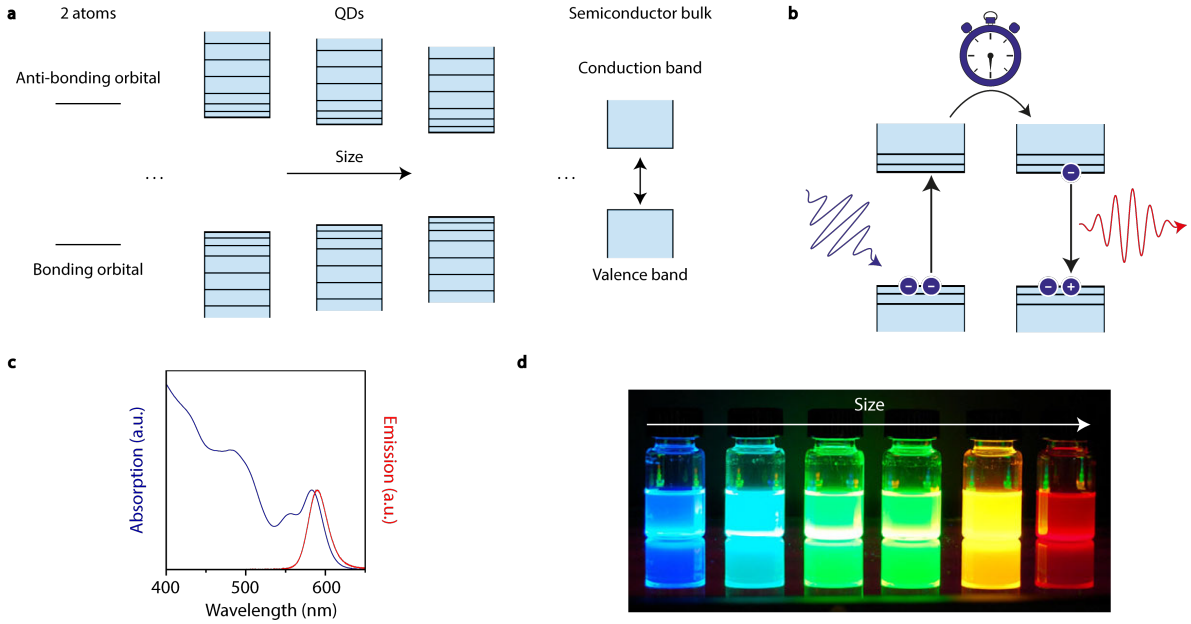

Figure 2.1: Electronic structure of QDs and its interaction with light. (**a**) A chemical bond between two atoms forms an anti-bonding and a bonding molecular orbital separated in energy. Combining many atoms in a crystal results in an anti-bonding energy band called the conduction band and a bonding energy band called the valence band, separated by the bandgap energy. QDs are in between these to limits since the amount of atoms is small. (**b**) Light in the visible or UV can be used to excite an electron from the valence band to the conduction band. The excited electron will form a bound state called an exciton with the hole it left behind. After some time the electron and hole will recombine emitting a photon matching the bandgap energy of the QD. (**c**) Absorption and emission spectrum of CdSe QD showing the wide absorption features and the narrow emission width. (**d**) Rainbow of emission colours by tuning the size of CdSe QDs (copied from Sigma-Aldrich).

In 1993 Murray et al. were the first to achieve highly mono-disperse QD samples. However, the chemical stability and optical performance of the QDs were still poor. A lot of effort was put into improving these properties over the years. A common approach to improve both these properties is growing a protective shell around the luminescent core consisting of a different material like CdS or ZnS.[15, 16] Depending on the core and shell materials used the delocalization of the excited electron and hole wavefunction throughout the QD will be different.
Figure 2.2 (**a**) shows Type 1 QDs, for example CdSe/ZnS, CdS/ZnS or InP/ZnS. The

bandgap of the core material in these types of QDs is smaller than the bandgap of the shell material thereby effectively confining electron and hole wavefunction to the core. The wavefunctions of the core/shell system are obtained by variational theory with particle-in-a-spherical-well functions as basisfunctions. The wavefunctions in figure 2.2 are the lowest-energy single particle state wavefunctions for the electron and the hole called the 1Se/h wavefunctions. For Type 2 QDs, for example CdTe/CdSe, CdSe/ZnTe or ZnSe/CdS both the conduction band and valence band edges are shifted up with respect to the shell material. Therefore, the electron will mainly be confined in the shell material and the hole mainly in the core as can be seen in figure 2.2. A reduction in spatial overlap between the hole and electron wavefunctions will reduce the rate of recombination and therefore we can expect that the time between excitation and emission will be larger than for Type 1 QDs. The last type of QDs is called Quasi-type 2 QD, since they are in between type 1 and type 2. A well known example of this type of QD is CdSe/CdS or CdSe/CdS/ZnS which will be the main studied QD samples throughout this thesis. The band alignment between core and shell material is slightly asymmetric. Therefore, the hole will be largely confined to the core while the electron can delocalize to the shell material. Because of this spatial separation of charge carriers, we can expect again longer times for the exciton to recombine. Additionally, because delocalization of the electron wavefunction inside the shell decreases quantum confinement the emission will red-shift compared to the core-only emission.[12]

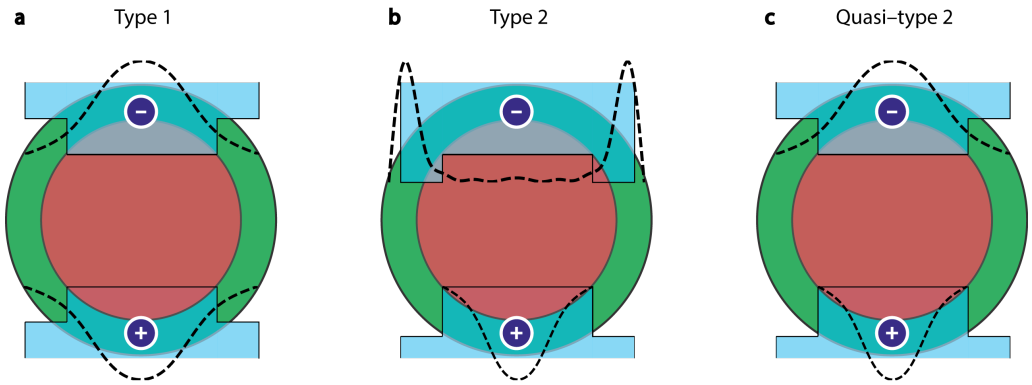

Figure 2.2: Wavefunction inside core/shell QDs. (**a**). Type 1 QDs where the bandgap of the core material lies completely inside the shell material band gap. Both electron and hole wave functions are confined to the core. (**b**) Type 2 QDs where the conduction band and valence band edges are shifted up with respect to the shell material. Therefore, the electron wavefunction is mainly located in the shell and the hole wavefunction is located in the core. (**c**) Quasi-type 2 QDs where only the electron wavefunction is delocalized throught the entire core/shell QD. All lowest-energy exciton state wavefunctions drawn are calculated based on variational theory using the first 10 particle-in-a-spherical-well functions by introducing a potential difference between the core material and shell material. We assume equal effective mass of the electron and the hole.

2.1.1 Decay dynamics of quantum dots

In the previous section we saw that by exciting QDs with light we can generate excitons that delocalize inside the QD. We stated that after some time the electron and hole recombine again thereby emitting a photon. In terms of the quasi-particle we can say that the exciton decayed. Here, we will investigate how we can study the time dynamics of these decays. Experimentally, decay dynamics of QDs are studied by excitation with a laser pulse which is short on the timescale of the decay. In this thesis we use pulsed excitation with a constant time between laser pulses. Typically an exciton in CdSe/CdS QDs decays within 20 ns after excitation. After every laser pulse we start a virtual stopwatch and when we detect a photon we stop it again. The time between these two events is called the delay time.

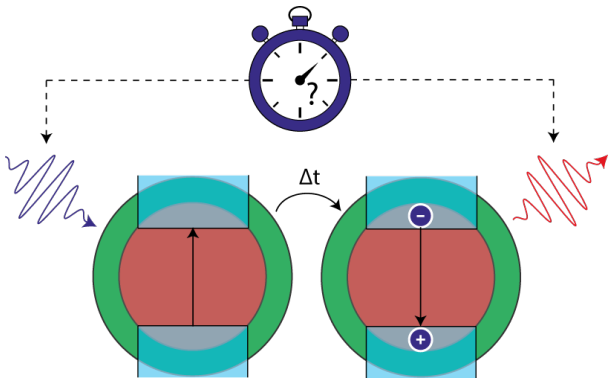

Figure 2.3: Schematic overview of decay dynamics measurements. Experimentally, a stopwatch will detect the delay time between an excitation pulse, which has a short duration with respect to the decay, and the emitted photon.

Throughout this thesis we will consider direct emission from QDs as a decay process between two energy levels. By excitation of a QD sample by a laser pulse we will excite a fraction of the QDs. We can model the decay of all these QDs by considering them as identical copies. Together with the rate constant describing the decay we can write the change of the number of QDs in the excited state per unit time

$$\mathrm{d}N = -N \sum_i \gamma_i \mathrm{d}t, \tag{2.1}$$

where we assume that the change is proportional to the number of excited QDs multiplied by all the processes by which the QD can relaxate to the ground state. The sum of decay rates can be split into two fundamentally different processes. We distuinguish between **radiative** processes that emit light and **non-radiative** processes that do not emit light. Exciton decay by non-radiative processes typically transfers it energy to either lattice phonons of the QD (heat) or by transferring its energy to other charge carriers (Auger decay). Assuming that there can be a multitude of different radiative and non-radiative processes in a QD sample, we can write for the total decay rate

$$\Gamma = \sum_i \gamma_{\mathrm{r},i} + \sum_i \gamma_{\mathrm{nr},i} = \Gamma_\mathrm{r} + \Gamma_\mathrm{nr}, \tag{2.2}$$

where Γ_r and Γ_nr are the total radiative and non-radiative rates and $1/\Gamma$ is equal to the lifetime of the exciton. We can integrate the expression above on the interval $[0, t]$ to obtain the number QDs in the excited state at time t. We obtain

$$N(t) = N(0)\mathrm{e}^{-\Gamma t}, \tag{2.3}$$

where $N(0)$ is the number of QDs in the excited state directly after excitation, which is proportional to the intensity of the laser and the absorption cross section σ_{abs}. In an experiment, we detect light emitted by QDs in radiative processes. Therefore we can write for the intensity we collect in our experiment

$$I(t) = \Gamma_r N(0) \eta \mathrm{e}^{-\Gamma t}, \tag{2.4}$$

where the intensity we observe for every delay time is linearly proportional to the total radiative decay rate and the collection efficiency η. Interestingly, although in our experiments we only detect light emitted by radiative processes, we also observe the non-radiative processes in the exponential decay. To define a good measure for the efficiency of the QDs we look at the integral over all detected photons

$$\int_0^\infty I(t)\mathrm{d}t = \frac{\Gamma_\mathrm{r}}{\Gamma_\mathrm{r} + \Gamma_\mathrm{nr}} N(0)\eta. \tag{2.5}$$

This shows that the fraction of decayed excitons which are observed in experiment is given by $\frac{\Gamma_\mathrm{r}}{\Gamma_\mathrm{r}+\Gamma_\mathrm{nr}}$ which is called the quantum yield (QY) of the QD emission.

2.1.2 Statistical scaling

In this thesis, we will change the emissive state of QDs by adding electrons to the 1Se energy level. This can be done either by photodoping where a photodoping agent, for example Li[Et_3BH], abstracts a hole after exciton formation or by electrochemical charging where the QDs are in electrical contact with an external electron reservoir.[17, 18] The latter will be used in chapter 5 of this thesis.
Here, we will explain what changes in the absorption and emission characteristics of colloidal QDs when additional electrons are present in the 1Se energy level based on simple statistical scaling arguments.[19] We denote neutral QDs in the ground state by G^0 figure 2.4 (**a**), where zero electrons are present in the 1S energy level. From the ground state G^0, light can be absorbed by the QD and an uncharged exciton X^0 is formed. This uncharged exciton will decay with a rate γ^{X^0} equal to the radiative rate $\gamma_\mathrm{r}^{X^0}$. For a radiative rate of 1/20 ns we expect a PL decay curve normalized to the number of QDs in the excited state as can be seen in figure 2.4 (**d**), where the amplitude is equal to the radiative rate as explained above.
By adding an electron to the 1Se energy we will obtain a singly charged QD in the ground state, which we denote by G^-. Since there is already an electron present in this charged ground state, only half of the light can be absorbed by the QD compared to the uncharged QDs as schematically depicted in figure 2.4 (**b**). This phenomenon is called absorption bleach and experimental results on this are shown in chapter 5. Absorption of light by charged QDs will generate a charged exciton X^-, also called a trion. This additional electron in the singly charged exciton will influence both the radiative and the non-radiative processes. The radiative rate of the charged exciton is twice the radiative rate of an uncharged, e.g. $\gamma_\mathrm{r}^{X^-} = 2\gamma_\mathrm{r}^{X^0}$, because the hole can recombine with two instead of one electron. The additional electron will also introduce non-radiative Auger processes since both electrons can recombine with the hole and transfer their energy to the electron that stays behind with a Auger rate γ_A. The total non-radiative rate therefore is $\gamma_\mathrm{nr}^{X^-} = 2\gamma_\mathrm{A}$, since both electrons can non-radiatively recombine with the hole. Based on the

higher radiative rate and the introduced non-radiative rate we expect several changes in the PL decay curve. Firstly, the higher radiative rate results in a higher amplitude of the decay curve as can be seen in figure 2.4 (**e**). Additionally, the introduced non-radiative processes increase the decay rate of the charged exciton and lowers the QY of the QDs. If we assume a non-radiative Auger rate of 1/10 ns, we expect a PL decay curve shown in figure 2.4 (**e**), where the total decay rate $\gamma^{X^-} = 2\gamma_r^{X^0} + 2\gamma_A = 3/10$ ns and the QY is only 33 %.
Since the 1Se energy level is doubly degenerate we can add another electron to the QD, we denote this doubly charged ground state G^{2-}. Because with 2 added electrons the 1Se energy level is completely filled, we expect a complete absorption bleach of the 1S absorption as schematically depicted in figure 2.4 (**c**). However, higher energy light can be absorbed which excites an electron to the 1Pe energy level, which lies in energy above the 1S energy level. A doubly charged exciton, sometimes called a tetron, will be formed, which we denote by X^{2-}. Addition of two additional electrons will change again the radiative and the non-radiative rates. Because of the same statistical argument used for the singly charged excitons, the doubly charged excitons will have a radiative rate of $\gamma_r^{X^{2-}} = 3\gamma_r^{X^0}$. For the non-radiative rate of the doubly charged exciton the same statistical extension can be used where the non-radiative rate becomes $\gamma_{nr} = 6\gamma_A$. If we assume again a non-radiative Auger rate of 1/10 ns, we expect a PL decay curve shown in figure 2.4 (**f**), where the total decay rate $\gamma^{X^{2-}} = 3\gamma_r^{X^0} + 6\gamma_A = 3/4$ ns and the QY further decreased to only 20 %.
In this thesis we will test this statistical scaling of the decay rates by electrochemically charging a QD film consisting of CdSe/CdS/ZnS QDs in chapter.

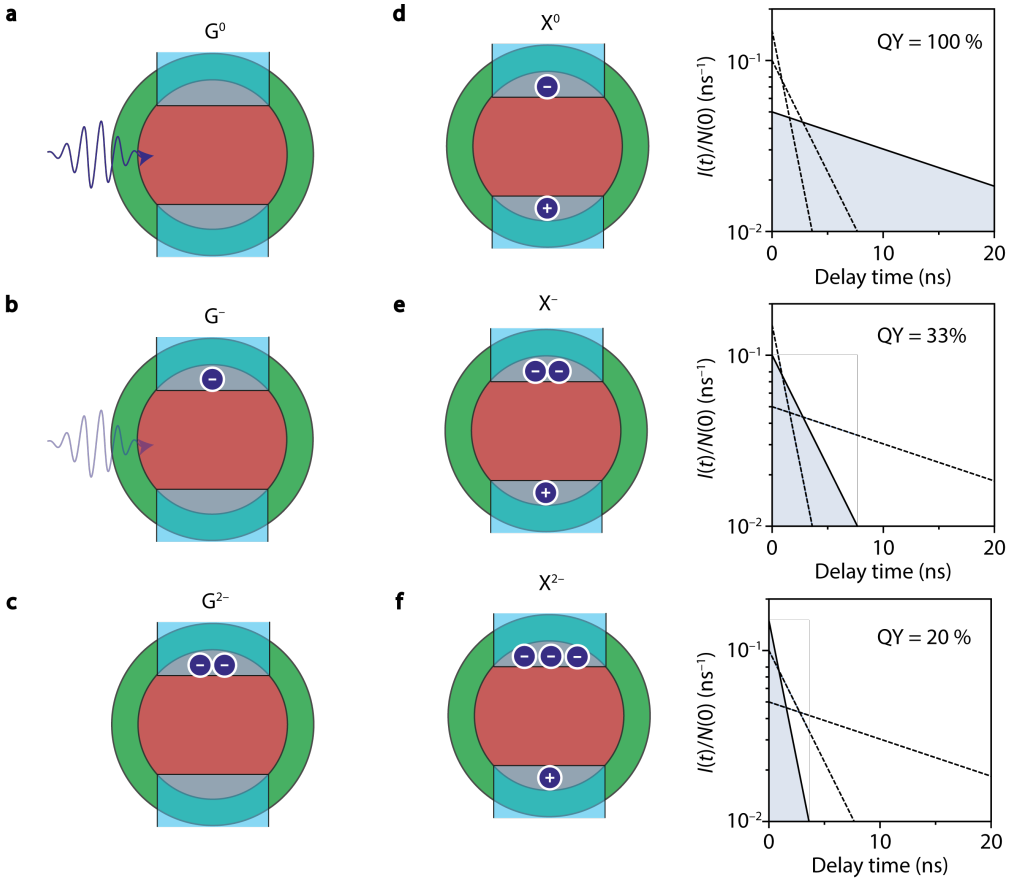

Figure 2.4: Statistical scaling of recombination rates in QDs. (**a**) Uncharged QD in the ground state where resonant light can be absorbed to promote an electron to the conduction band. (**b**) An singly charged QD in the ground state G^{-}, where less light can be absorbed by the 1S absorption since already one 1S energy level is occupied. This effect is called absorption bleach. (**c**) Doubly charged QD in the ground state G^{2-} shows no 1S absorption any more and this transition is completely bleached. (**d**) Neutral exciton X^0 with a radiative rate $\gamma_r^{X^0}$ of 1/20 ns, corresponding decay curve on the right shows mono-exponential decay with a lifetime of 20 ns. The area under the decay curve is equal to the QY and is 100 %. (**e**) Singly charged excitons X^{-} having one additional electron in the conduction band in the excited state. Decay curve on the right shows a higher amplitude because $\gamma_r^{X^-} = 2\gamma_r^{X^0}$. The total decay rate γ^{X^-} is shorter, e.g. $\gamma^{X^-} = 3/10$ ns, because of the additional Auger rates, where γ_A is 1/10 ns. (**f**) Two additional electrons in 1S energy level changes the amplitude even more since $\gamma_r^{X^{2-}} = 3\gamma_r^{X^0}$. The total decay rate $\gamma^{X^{2-}}$ is now much shorter, e.g. $\gamma^{X^{2-}} = 3/4$ ns.

2.2 Delayed emission and its relation to trap states

As discussed earlier in the introduction, delayed exciton emission is commonly attributed to trapping and subsequent release of charge carriers. Radiative charge carrier recombination after release results in photon emission relatively long after pulsed excitation. In this section an overview is given of some existing models which could possibly explain delayed exciton emission followed by a discussion about the chemical identity of the trap states.

2.2.1 Distributed kinetics of trapped charge carriers

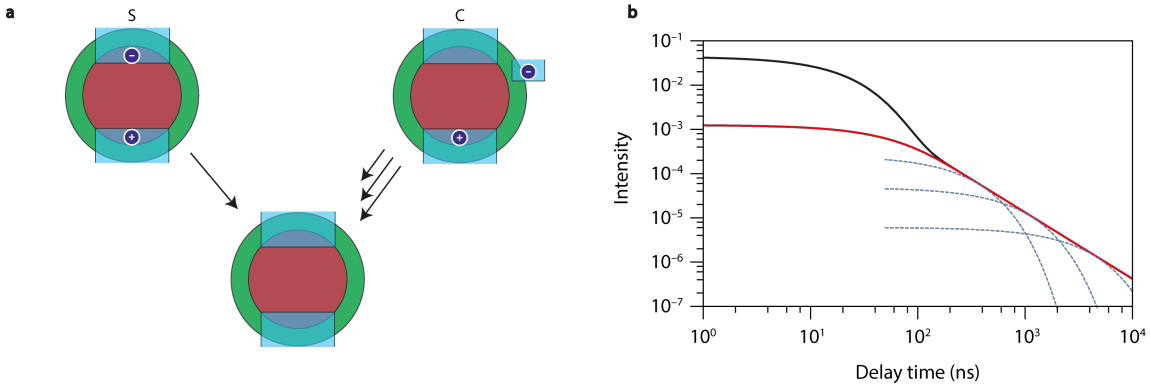

Figure 2.5: Distribution of release rate model for delayed emission. (**a**) In this model, the probability of temporary charge carrier trapping to a meta-stable charge separated state C is P_S. Relaxation to the ground state goes via a distribution of release rates. From state S, $1 - P_S$ relaxates to the ground state via a single direct emission rate. (**b**) Modelled decay curve (black) for a radiative decay rate of 1/20 ns, a trapping probability of 15 % and a power-law exponent $\alpha = 1.5$. The curve in red shows the part of the emission which is due to delayed emission and the dashed insets are single exponential rates contributing to the power-law decay. Adapted from [11].

Delayed exciton emission can generally be recognized experimentally as having highly non-exponential decay dynamics. The two models explained below try to explain this non-exponential decay by assuming that the release is slow and has a broad distribution in kinetics. The first model by Rabouw et al. models the delayed exciton emission by assuming a powerlaw distribution of release rate and the second model by Marchioro et al. assumes that trapped charge carriers need to tunnel back to an emissive state, where the tunneling barriers vary.[20, 11, 5]

Figure 2.5 (**a**) shows the hypothesized model contributing to delayed exciton emission where after formation of an exciton, there is a probability of trapping to a meta-stable charge seperated state C. We assume that release of the trapped charge carriers is broadly distributed following a power-law distribution, $\rho(\gamma) = \gamma^{\alpha-2}$, where γ is the variable release rate and α is the power-law exponent. From this we calculate the total amount of delayed emission by integrating over all possible release rates with

$$I_{\mathrm{d}}(t) \propto \int_0^{\gamma_{\max}} \mathrm{d}\gamma\gamma\rho(\gamma)\mathrm{e}^{-\gamma t}, \tag{2.6}$$

where the extra factor γ accounts for the proportionality between the population of trapped charges and the observed intensity. The upper limit $\gamma_{\max}$ of the integral is introduced to avoid singularities in the integration, where I_{d} will diverge for γ going to infinity. Setting the upper limit to half the exciton recombination rate, e.g $\gamma_{\max} = \gamma_{\mathrm{X}}/2$, gives

$$I_{\mathrm{d}}(t) = \frac{\alpha - 1}{(\gamma_{\mathrm{X}}/2)^{\alpha-1}} t^{-\alpha} \left(\Gamma(\alpha) - \Gamma\left(\alpha, \frac{\gamma_{\mathrm{X}} t}{2}\right)\right). \tag{2.7}$$

This upper limit arises because even for extremely fast release rates, the QD goes twice through the exciton state S with a lifetime of $1/\gamma_{\mathrm{X}}$. With a probability of trapping of P_{S}, we obtain for the total emission intensity,

$$I_{\mathrm{d}}(t) = (1 - P_{\mathrm{S}})\gamma_{\mathrm{X}}\mathrm{e}^{-\gamma_{\mathrm{X}} t} + P_{\mathrm{S}} \frac{\alpha - 1}{(\gamma_{\mathrm{X}}/2)^{\alpha-1}} t^{-\alpha} \left(\Gamma(\alpha) - \Gamma\left(\alpha, \frac{\gamma_{\mathrm{X}} t}{2}\right)\right). \tag{2.8}$$

Figure 2.5 (**b**) shows the modelled decay curve of direct and delayed exciton emission in black (Trapping probability $P_{\mathrm{S}} = 15$ %), where the exciton recombination rate $\gamma_{\mathrm{X}} = 1/20$ ns and the power-law $\alpha = 1.5$. The delayed emission part of the emission is shown in red and the three dotted single-exponential curves (from left to right $\gamma = 1/250$ ns, 1/750 and 1/3000 ns) show part of the power-law distribution of release rate giving rise to this broad distribution.

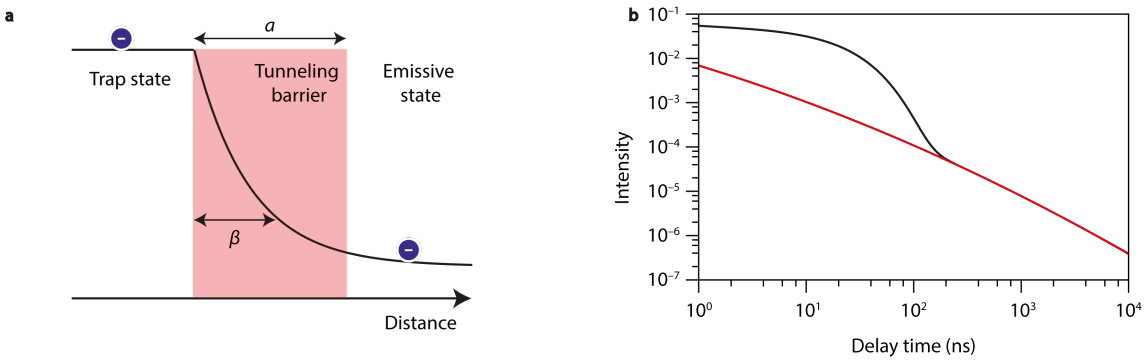

Figure 2.6: Tunneling model for delayed emission. (**a**) Trapped charge carriers can tunnel back to the emissive state through a tunneling barrier of width a and tunneling decay constant β, a distribution of tunneling widths will give rise to distributed kinetics. (**b**) Modelled decay curve based on the tunneling parameters $\gamma_X = 1/20$ ns, $\langle a \rangle = 1$, $k_0 = 10^9$ ns^{-1}, $\sigma = 0.3$ and $\beta = 12$. Although the total modelled curve (black) looks approximately the same as for the distribution of release rate model, the delayed emission part (red) for low delay times has a higher amplitude compared to the model by Rabouw et al.[10]

The second model by Marchioro et al. explains the distributed kinetics of delayed exciton recombination by tunneling of trapped charge carriers to the emissive exciton state, see figure 2.6 (**b**). Motivation for this slightly different model comes from temperature dependent PL decay measurements of CdSe, Cu^+:CdSe and $CuInS_2$, where they showed that delayed emission dynamics did not change from 20 K to room temperature indicating a temperature-independent tunneling mechanism.[10] If we start out in the metastable charge-separated state, there is a chance to go back to the emissive state by tunneling with a rate

$$k(a) = k_0 \mathrm{e}^{-\beta a}, \tag{2.9}$$

where β is the tunneling decay constant, a is the width of the barrier and k_0 is the tunneling rate when no barrier is present. To obtain distributed kinetics with temperature independent tunneling rate we assume a Gaussian distribution $p(a, \langle a \rangle, \sigma)$ of tunneling barriers around an average tunnel width $\langle a \rangle$. The total emission intensity can be calculated by

$$I(t) = A_\mathrm{p} \mathrm{e}^{-\gamma_X t} + A_\mathrm{d} \int_0^\infty \mathrm{d}a p(a) \mathrm{e}^{-k(a)t}, \tag{2.10}$$

where A_p and A_d are the prompt and delayed emission amplitudes. This integral can be solved numerically for a set of tunneling parameters. Figure 2.6 (**d**) shows a decay curve based on this model for $\gamma_X = 1/20$ ns, $\langle a \rangle = 1$, $k_0 = 10^9$ ns^{-1}, $\sigma = 0.3$ and $\beta = 12$. Inspection of figures 2.6 (**b**) 2.5 (**b**) and shows almost similar total emission decay curves for the tunneling model by Marchioro et al. and the release rate model by Rabouw et al. Motivation to use this tunneling model by Marchioro was that it produces a deviation from power-law decay consistent with experiment.
The two models explain the distributed kinetics observed in ensemble PL decay curves and fit the experimental data well. However, the microscopic origin of charge carrier

trapping and release is still unclear. The distributed kinetics could be explained by two scenarios, either 1) ensemble averaging gives distributed kinetics, e.g. every QD has one fixed release rate or tunneling barrier and only together they would give distributed kinetics in the overall PL decay. In an alternative scenario 2) every QD already shows either a distribution of release rates or a distribution of tunneling barriers. If scenario 2) is observed for single QDs, experiments on the decay dynamics over time could shed some light on the temporal characteristics of delayed emission. Perhaps release rates or tunneling barriers are dynamic and fluctuate significantly in experiments on single QDs. Observation of either of the two scenarios is masked in ensemble experiments by averaging. Only experiments on delayed emission of single QDs can answer these questions, showing the necessity of this technique in shedding light on this phenomenon.

2.2.2 Diffusion of trapped charge carriers

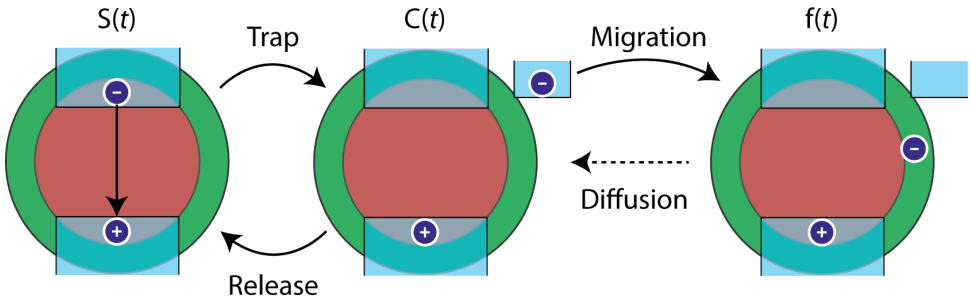

Figure 2.7: Diffusion model of trapped charge carriers. After excitation of the colloidal QD two processes are in competition. The charge carrier can radiatively recombine from S(t)and emit a photon or trapping of the charge carrier to state C(t) can occur. From this metastable charge-separated state the charge can migrate with a rate γ_S to state f(t) after which 3D diffusion is the process that transports the charge back to the charge-separated state. Release of the trapped charge via the meta-stable state C(t) will result in delayed exciton emission with characteristic power-law decay.

The models discussed previously showed that decay dynamics of delayed exciton emission can be modelled by assuming a broad distribution of release rates. Here, an overview of a different kind of model will be given where diffusion of trapped charges gives rise to power-law decay. The model on which this derivation is based was used to describe delayed emission in molecular crystals where organic molecules could switch from a singlet to two non-fluorescent triplet states.[21] These triplet states can separate through migration in the crystal. When two triplets meet again they can form a fluorescent singlet state and emit a photon. Although this is a completely different system, people have used the same model in similar systems compared to CdSe, like CdS non-uniform nanorods, to explain power-law decay in transient absorption measurements.[22]
Figure 2.7 shows a schematic overview of the diffusion model. On the left the lowest-energy exciton state $S(t)$ is given, from here a charge carrier can be trapped with a rate γ_T to the meta-stable charge separated state $C(t)$. Now, the trapped charge can be either released by a rate γ_R or the trapped charge can instantaneously migrate with a rate γ_M to a different trap state $f(t)$ from where release is impossible. By diffusing through trap

states the charge carrier can migrate back to the charge separated state where release is possible again. The differential equations describing this model are given by

$$\begin{aligned}\frac{\partial S(t)}{\partial t} &= -(\gamma_{\mathrm{X}} + \gamma_{\mathrm{T}})S(t) + \gamma_{\mathrm{R}}C(t) \\ \frac{\partial C(t)}{\partial t} &= \gamma_{\mathrm{T}}S(t) - (\gamma_{\mathrm{R}} + \gamma_{\mathrm{M}})C(t) + \gamma_{\mathrm{D}}(t) \\ \frac{\partial f(t)}{\partial t} &= \gamma_{\mathrm{M}}C(t) - \gamma_{\mathrm{D}}(t),\end{aligned} \tag{2.11}$$

where γ_{T} and γ_{R} are the trapping and release rates, γ_{X} is the exciton recombination rate,γ_{M} is the migration of trapped charge to a trap state where no release is possible and γ_{D} is the time-dependent diffusion rate of the charge back to the charge separated state. The time-dependent diffusion rate can be calculated by

$$\gamma_{\mathrm{D}}(t) = \gamma_{\mathrm{M}} \int_0^t \mathrm{d}t_1 P(b, t - t_1)C(t_1), \tag{2.12}$$

where the separated charge can migrate between zero and a time t proportional to the population of the charge separated state and the migration rate (e.g. $\gamma_{\mathrm{M}}C(t)$). The function $P(t-t_1)$ is called the regeneration kernel and physically it gives the time distribution of regeneration of a migrated charge. In 3D this can be given by the diffusion equation which is given by

$$P(b, t) \propto \frac{1}{t^{3/2}} \exp(-b^2/4Dt), \tag{2.13}$$

where b is the distance between the migrated charge and the charge separated state and D is the diffusion coefficient of the charge through the colloidal QD.[23] To solve this linear system of differential equations it is convenient to perform a Laplace transformation to get rid of the time-derivatives. The Laplace transform of the top two differential equations give

$$\begin{aligned}s\hat{S}(s) - S(0) &= -(\gamma_{\mathrm{X}} + \gamma_{\mathrm{T}})\hat{S}(s) + \gamma_{\mathrm{R}}\hat{C}(s) \\ s\hat{C}(s) - C(0) &= \gamma_{\mathrm{T}}\hat{S}(s) - (\gamma_{\mathrm{R}} + \gamma_{\mathrm{M}})\hat{C}(s) + \gamma_{\mathrm{M}}\hat{P}(s)\hat{C}(s),\end{aligned} \tag{2.14}$$

where we used that the Laplace transform of a time derivative is given by $(\mathcal{L}\dot{f}(t)) = s\hat{f}(s) - f(0)$, which follows from partial integration. We assume that directly after excitation no charges are separated yet and therefore $C(0) = 0$. Additionally, we assume that trapping γ_{T} and release γ_{R} is equal and from now on given by γ. We can now solve for the population of the lowest-energy exciton state given by

$$\frac{\hat{S}(s)}{S(0)} = \left[s + \gamma + \gamma_{\mathrm{X}} - \frac{\gamma^2}{s + \gamma + \gamma_{\mathrm{M}}(1 - \hat{P}(s))} \right]^{-1}. \tag{2.15}$$

Here, the population of the exciton state is given as a function of all the rates in this kinetic model. For the Laplace transform of the regeneration kernel we obtain

$$\hat{P}(s) \propto \int_0^\infty \mathrm{d}t e^{-st} \frac{1}{t^{3/2}} \exp(-b^2/4Dt) \propto \exp(-b\sqrt{s/D}). \tag{2.16}$$

to observe the influence of diffusion of migrated trapped charges on the decay dynamics we consider the low migration rates s which correspond to long times t after excitation. In this limit the population of the lowest-energy exciton state simplifies considerably since we can Taylor expand the regeneration kernel, e.g. $1 - \hat{P}(s) \approx b\sqrt{s/D}$. To first order in $\sqrt{s/D}$ this gives

$$\frac{\hat{S}(s)}{S(0)} = \left[\gamma + \gamma_\mathrm{X} - \frac{\gamma^2}{\gamma + \gamma_\mathrm{M} b \sqrt{\frac{s}{D}}}\right]^{-1} \approx \frac{1}{2\gamma + \gamma_\mathrm{X}} - \frac{\gamma_\mathrm{M} b}{(2\gamma + \gamma_\mathrm{X})^2}\sqrt{\frac{s}{D}}. \tag{2.17}$$

If we assume that migration from the charge-separated state $\mathrm{C}(t)$ is fast and diffusion back to the charge-separated state $\mathrm{C}(t)$ is slow compared to trapping and excitation recombination, e.g. $\gamma_\mathrm{M} b\sqrt{s/D} \gg 2\gamma + \gamma_\mathrm{X}$, we can neglect the first term. We can finally perform a inverse Laplace transform which gives

$$\frac{S(t)}{S(0)} \approx \frac{\gamma_\mathrm{M} b}{2(2\gamma + \gamma_\mathrm{X})^2} \frac{\sqrt{\pi}}{\sqrt{D} t^{3/2}} \propto t^{-3/2}. \tag{2.18}$$

So indeed, assuming that we have diffusion of migrated trapped charges in the colloidal QDs gives power-law decay at large time delays! Interestingly even the analytically obtained value for the power-law exponent α is close to what people commonly measure for colloidal QDs. This model can be extended to quantum systems where diffusion is limited to either 2D or even 1D. Here, decay is expected to follow a power-law decay with exponent $\alpha_\mathrm{2D} = 1$ and $\alpha_\mathrm{1D} = 1/2$. Earlier work by Rabouw et al. shows on CdSe nanoplatelets that this dimensional scaling does not hold.[20] In these systems delayed emission with a power-law exponent $\alpha = 2.1$ is found. This might indicate that regeneration kernels based on a simple diffusion equation breaks down and that additonal influences like electrostatic effects need to be included.

2.2.3 Origin of trap states

Above, several models have been shown by which delayed emission of an exciton can be explained. Although experimental data and the models show great resemblance, the origin of trap states remains unclear. People generally assume that trap states result into a lower QY because of non-radiative processes. Observation of delayed emission proves that trapping of excited charge carriers can also be reversible. Here, we will give some hypothesized origins of charge carrier trapping which may contribute to delayed emission. The first origin of trap states in colloidal QDs are surface defects. Both core-only and core/shell QDs have a capping layer of ligands which keeps them colloidally stable in a solvent, either by entropic or electrostatic repulsions. Complete stripping of the ligands will result in aggregation of the nanoparticles. However, QDs remain colloidally stable despite ligands missing. Theoretical calculations show that uncoordinated surface atoms can result in trap states for excited charge carriers. An article by Kirkwood et al. shows by performing density function theory (DFT) calculations that uncoordinated anions on the surface of CdTe, CdSe, InZnP and CdS QDs gives rise to trap states with an energy inside the bandgap.[24] Treatment of these materials with a salt, for example $InCl_3$

or $CdCl_2$, shows a significant increase of the QY which shows that these uncoordinated surface atoms contributed to non-radiative processes. Other work by Baker et al. and Kalyuzhny et al. show that tuning the decay dynamics of CdSe QDs is possible by exchanging the capping ligands by other types of ligands.[25, 26] Both show that direct emission from surface trap states is possible, by observing a red-detuned emission band alongside the exciton emission.
A second type of defects in core/shell QDs originates from strain between the luminescent core and passivating shell (for example ZnS or CdS). The difference between the crystal lattices of CdSe and the shell material will cause strain at the core/shell interface. Research by Creti et al. on CdSe cores and CdSe/CdS/ZnS nanorods shows that growing of the CdS/ZnS shell introduces additional trap states.[27] The core/shell nanorods show photoinduced absorption in transient transmission measurements. This absorption, which is only observed for the core/shell system, is attributed to trapped electrons in trap states inside the bandgap. Strain defects between the core and shell are given as a possible explanation for the trap states. A possible solution to solve strain defects in core/shell QDs is by growing the shell at high temperatures with a slow dropwise addition of the precursors. This synthesis method introduced by Boldt et al. produces a graded-shell alloy which minimizes the strain between the core and shell materials.[16]
Above discussion shows that much can be learned about the origin of trapping in colloidal QDs. Non-radiative processes, trap-state emission and delayed exciton emission are all processes that can be observed in this sytem indicating a plethora of different kinds of trap states. Which trap states contribute to delayed emission remains unclear and hopefully this thesis will contribute to this discussion.

Chapter 3

Method

3.1 Single QD measurements

3.1.1 QD synthesis

Materials
CdO (99.99%), Cd(II)-acetate (99.995%), Zn(II)-acetate (99.99%), Octadecene (ODE, 90%), Oleylamine (OLAM, 99.8%), Oleic acid (OA, 90%), Butanol (BuOH, Anhydrous, 99.8%), Methanol (MeOH, Anhydrous, 99.8%), Hexane (99.8%, Anhydrous), Octadecylphosphonic acid (ODPA, 97%), Trioctyl phosphineoxide (TOPO, technical grade, 90%), Trioctylphosphine (TOP, 97%), 1-Octanethiol (>98.5%), Selenium powder (Se, 99.99%), and toluene (>95 %) all bought from Sigma-Aldrich. Chemicals were used as received unless specifically stated otherwise in the text below.

Core synthesis
The CdSe cores were synthesized based on a method reported by Carbone et al.[28] TOPO (3.000 g), ODPA (0.290 g) and CdO (0.060 g) were mixed in a 50 mL three-neck flask and degassed at circa 150 °C under vacuum for 2 hours. Under a nitrogen flow, the solution was heated to 320 °C. The solution turned clear and colorless under slow stirring (< 200 rpm) within 20 minutes which indicated the formation of Cd-ODPA complexes. 1.0 mL of TOP was injected when the solution became clear. To solution was heated to 370 °C and a TOP-Se solution (0.060 g Se in 0.500 mL TOP) was swiftly injected. The solution was kept at 350 °C for 1 minute to allow nanocrystal growth. After 1 minute, the reaction mixture was quickly cooled by using compressed air. At room temperature, 5 mL of toluene was injected. The nanocrystals were precipitated by methanol and collected by centrifugation. The nanocrystals were redispersed in toluene and the above steps were repeated three times. Finally, the nanocrystals were stored in a nitrogen-purged globebox.

Shell synthesis

Cd-oleate precursor

Cadmium acetate dihydrate (3.0 mmol, 0.801 g), oleic acid (6.00 mmol, 1.70 g) and ODE (31.15 mL) were mixed in a 50 mL three-neck flask to produce the cadmium oleate precursor. The solution was degassed for 4h at 100 °C under vacuum. Next, 2.0 mL (6.00 mmol, 1.61 g) of degassed OLAM was added to the solution to keep cadmium oleate stable in solution. The precursor was stored in a nitrogen-purged glovebox.

CdS shell growth

CdSe/CdS core/shell quantum dots (QDs) were prepared with CdSe cores of 4.1 nm in size, determined from absorption spectrum based on sizing curve by Yu et al. [29] Based on the core size the required amount of precursors was estimated. Each CdS layer was estimated to increase the radius by 0.141 nm.[30]

100 nmol of CdSe cores in toluene (concentration 60 μM), 3 mL of ODE, and 3 mL of oleylamine were mixed in a 50 mL three-neck flask in a nitrogen amosphere. The solution was degassed under vacuum for 45 minutes at 50 °C and 15 minutes at 120 °C. The temperature was slowly increased to 310 °C. Starting from 210 °C two separate solutions, cadmium oleate (1.48 mmol) in ODE (20 mL) and octanethiol (1.77 mmol) in ODE (20 mL), were injected dropwise with a rate of 2.5 mL/h. After the time it took to add the desired amount of precursor, the solution was cooled to 200 °C. Next, 1 mL of OA was added dropwise and the nanocrystal solution was kept at this temperature for 1 h to allowing annealing of the core and shell. The core/shell QDs were precipitated using a mixture of methanol/butanol. The QDs were collected after centrifugation at 1200 g for 10 min and redispered in hexane. These washing steps were repeated three times. The final product was dispersed in toluene and stored in a nitrogen-purged glovebox.

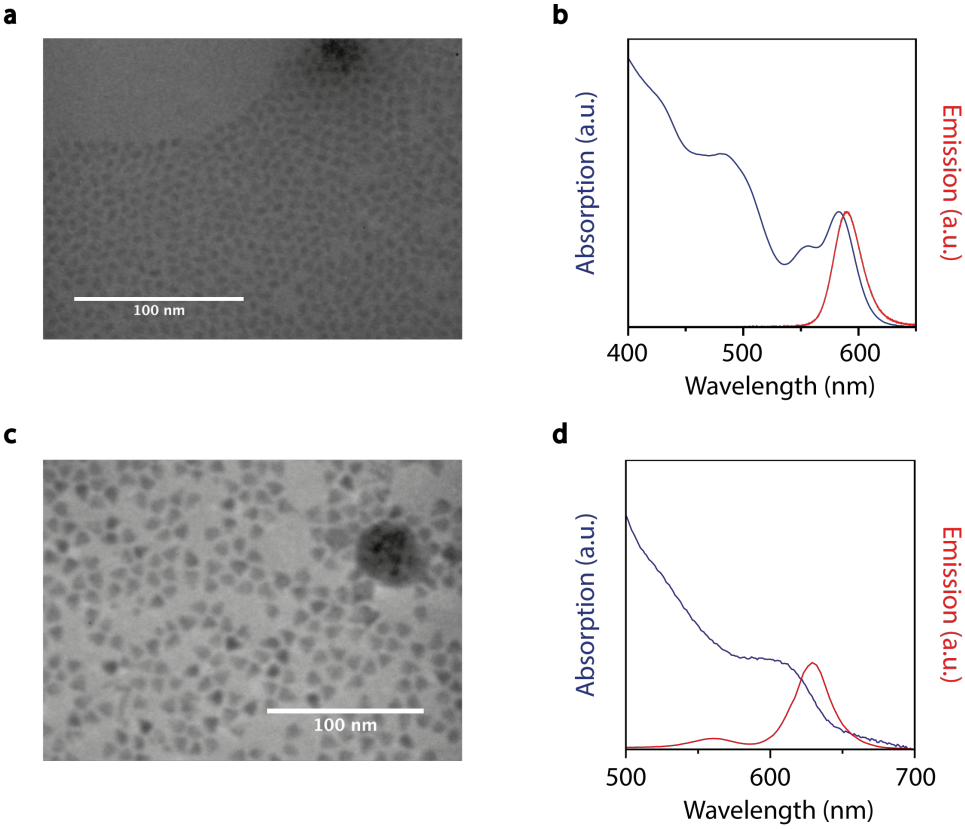

Figure 3.1: Characterisation of CdSe cores and CdSe/CdS core/shell QDs (**a**) TEM image shows CdSe cores with a size of 4.1 nm (size obtained from absorption spectrum). (**b**) PL emission maximum is at 595 nm. (**c**) TEM image shows CdSe/CdS with a size of 7.6 ± 0.2 nm obtained by averaging over 50 QDs in the sample. (**d**) The emission spectrum shows emission from secondary nucleation around 560 nm, the emission maximum is at 628 nm.

3.1.2 Single QD spectroscopy

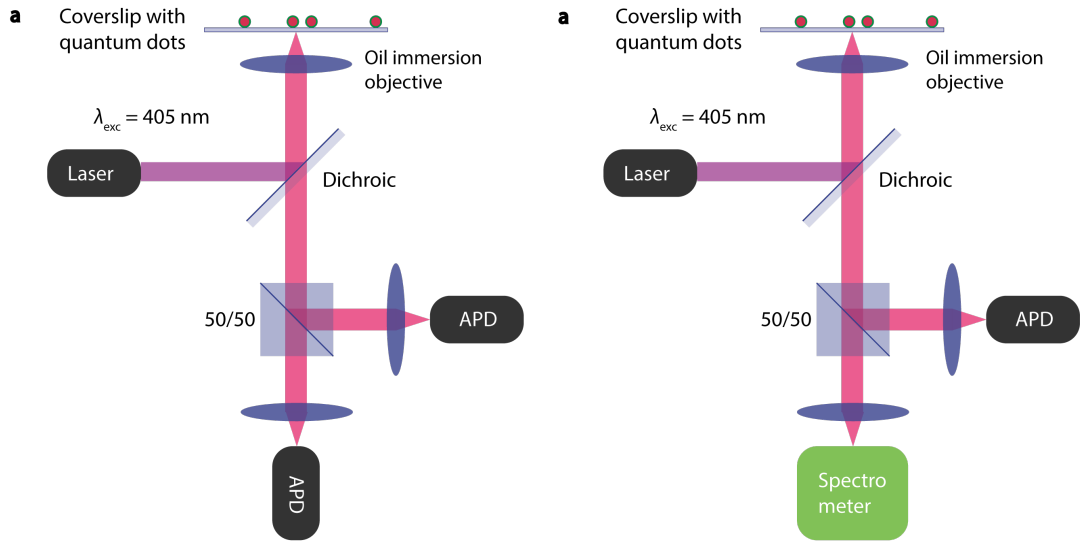

Figure 3.2: Schematic of single QD setup (**a**) Excitation by a 405 nm laser is reflected by a 520 dichroic mirror and focussed by an oil immersion objective on a coverslip. The emission light is collected through the same objective and split between two single photon avalanche photodiodes in a Hanbury Brown-Twiss setup. (**b**) Roughly the same experimental setup is used for the experiment measuring both decay dynamics and PL spectrum, however the emission light is split between a single photon APD and an EMCCD connected to a spectrometer.

Single QD measurements were performed by spin-coating QDs from a dilute dispersion onto a glass coverslip (#1.5, 0.17 mm thickness).
For the delayed emission experiments, single QDs were excited with a 405 nm Picoquant(P-C-405) laser with a fluence of 10 μJ/cm^2 (see Appendix A) and a repetition rate of 1 MHz. A 520 dichroic mirror is used to direct the excitation light to the oil-immersion objective (NA = 1.4). The laser beam diameter was cut-off with 3 mm iris to avoid over-filling of the objective. QD emission is collected through the same objective used for excitation. We used a Hanbury Brown-Twiss setup with two Picoquant PDM avalanche photodiodes (APDs, dark counts $<$ 5 Hz detector diameter of 20 μm) connected to a QuTools QuTAU timing box with a resolution of 81 ps. An additonal 700 nm short-pass filter was included before the beam splitter to minimize detection of afterglow from the APDs.
Experiments correlating delayed emission and the spectrum of single QDs were performed in a similar setup. However, emission light was split by a 50/50 beamsplitter, guiding 50 % to a PicoQuant APD (dark counts $<$ 5 Hz) and 50 % to an Andor Kimera 193i spectrometer in combination with a iXon EMCCD detector.

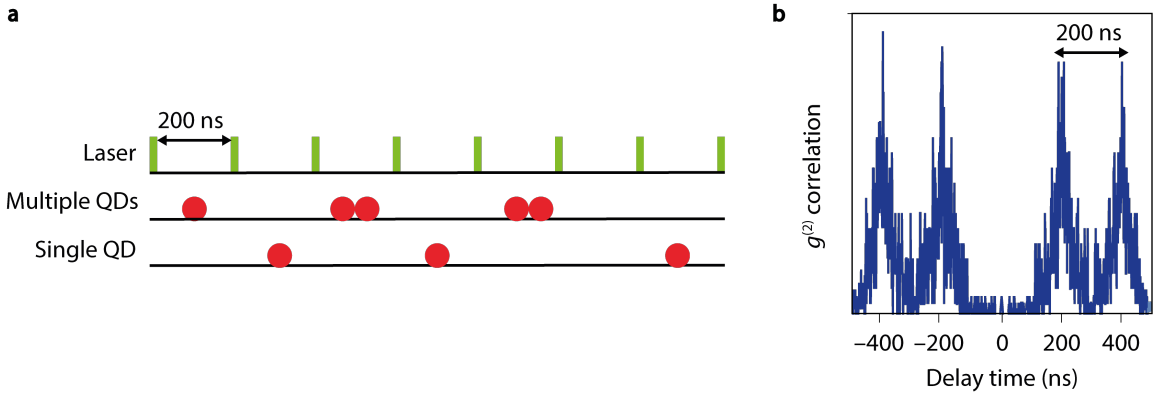

Figure 3.3: Cross correlations using a Hanbury Brown-Twiss setup. (**a**) Pulsed laser excitation with multiple QDs in the laser focus will have a significant probability of detecting multiple photons after a single laser pulse. If a single QD emitter is in focus, after every laser pulse only one photon can be detected. (**b**) Cross correlation between two single photon APDs calculates time delays between detection events on the two APDs. In a pulsed excitation experiment on a single emitter, time delays of zero are not present in the cross correlation function, this is called anti-bunching.

To verify in single QD experiments that we are measuring light emitted by a single QD, we use a Hanbury Brown-Twiss setup where the emission is split between two APDs by a beam splitter. We perform cross correlation between emission detected by the two APDs. Figure 3.3 (**a**) shows the pulse-train for a 5 MHz repetition rate experiment, e.g. time differences between laser pulses of 200 ns. In the situation where multiple QDs would be in our laser focus, the probability of detecting multiple photons after a single laser pulse is high. On the other hand, if we have just a single QD in our focus we can only detect one photon after a laser pulse. By calculating time delays between all photon pairs on APD 1 and APD 2 in a experiment we can distinguish the two scenarios described above. For every photon we detect on APD1 after pulse i, there is a probability to detect another photon on APD2 after pulse $i+1$ or $i+2$ etc. The probability of finding these photon pairs we observe in the second order correlation function as peaks at delay times of 200 or 400 ns, as can be seen in figure 3.3 (**b**). However, in the case where only a single emitter is present in the observation volume and we detect a photon on APD1 after pulse i, we will never observe a photon at APD2 after pulse i. This we can see from the second order correlation function as the absence of a peak at a delay time of zero, this effect is called anti-bunching and is used throughout this thesis to verify that a single emitter is in the observation volume. Experimentally we need two APDs because of the dead-time of approximately 100 ns after a detection event, thereby making it impossible to detect photon pairs with zero time delay.

APD characterisation

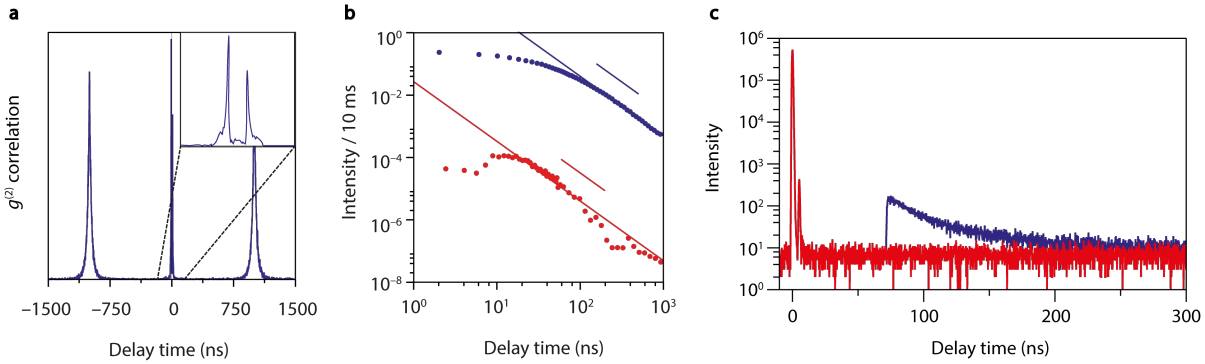

Figure 3.4: Afterglow and afterpulsing of single photon detectors. (**a**) A second order correlation function of an experiment using 1 MHz repetition rate, additional correlations are observed at delayed times $t = \pm$ 10 ns. These correlations likely arise from detector fluorescence, e.g. afterglow, initiated by a QD photon. The afterglow photon will travel back to the sample stage, is reflected on the coverslip and travels back to the other APD where it is detected. (**b**) A decay curve of an experiment on a single QD (blue). The decay curve of all afterglow photons (red) is merely a copy of the QD decay curve with an intensity roughly 10^4 smaller. The copy has an offset of approximately 10 ns because the afterglow photon first needs to travel to the sample stage and back to the other APD. (**c**) Decay curves of 405 nm laser reflections on a glass coverslip. Laser reflection decay within a few ns indicating the temporal width of the laser. An additional bump in the decay curve (blue) for $t > 80$ ns is due to afterpulsing events where the APD detects a non-existing photon. By discarding all second photons after a laser pulse, approximately all afterpulsing events are gone as can be seen in the correct decay curve (red).

Detectors used in single QD research require extremely good detection efficiency and low amount of dark counts. APDs can fulfil both these requirements. An incident photon generates an avalanche of charge carriers which leads to a detection event if the current exceeds a certain threshold. Here, we will characterise two unwanted side-effects of APDs: afterglow and afterpulsing. Afterglow is fluorescence of the detector materials and afterpulsing is the detection of non-existing photons. We will show how these features of APDs can be observed in our single QD experiments and how we can correct for them.

Afterglow

Incident QD photons on the detector area of a APD can result in detector fluorescence. This effect is called afterglow and has a broad spectrum ranging from 700 to 1100 nm.[31] Afterglow photons can travel all the way back to the sample stage where it is reflected on the glass coverslip and subsequently it can be detected by the other APD. This results in additional peaks in the second order correlation function as can be seen in figure 3.4 (**a**) at time delays of $t = \pm$ 10 ns, which is the time needed for light to travel from the APD to the sample stage and back again. To characterise these afterglow photons, we can construct the decay curve of only these photons, arriving always approximately 10 ns after a QD photon. The result is plotted in 3.4 (**b**), where we see the decay curve of

a single QD (blue) and the decay curve of afterglow photons(red). The afterglow decay curve is simply a copy of the QD decay curve with an intensity roughly 10^4 less. Due to this low intensity, misinterpreting afterglow photons with delayed emission photons is highly unlikely. However, possible precautions against afterglow could be taken. A short-pass filter of 700 nm in the detection path will filter out most of the afterglow photons. Another possibility is to match the refractive index of the medium above the coverslip with the refractive index of the coverslip. In this way, afterglow photons will not be reflected by the coverslip. The last option is a slight misalignment of one of the APDs to minimize the detection of afterglow photons.

Afterpulsing

APDs detect light by formation of an electric current when hit by a photon via the photo-electric effect.[32] Normally, one photon would only create one current that exceeds the detection threshold. However, there is a small probability (Picoquant APD used in this thesis: approximately 3 % [33]) where one photon generates a second current. This effect is called afterpulsing and results in additional photon detection events in a single QD experiment. Figure 3.4 (**c**) shows the decay curve of laser reflections from a 405 nm laser. The reflections decay very fast, within 1 ns, reflecting the temporal width of the laser. After approximately 80 ns the decay curve starts to rise again. This are all fake photon detection events caused by afterpulsing events by laser reflection photons. The decay dynamics of the afterpulsing events are highly non-exponential, therefore they can be possibly misinterpreted as delayed emission.

However, since we know that every afterpulse event is a reaction to a real photon, we can try to discard as many afterpulse events by discarding every second photon detection event after one laser pulse. As we can see in the red decay curve this completely eliminates the bump we observed earlier. However, a flat background remains that is approximately 1.5 % of the total intensity. We attribute this flat blackground to afterpulse events that are being detected as fake photons very long after the real photon. Therefore, they cannot be discarded by this technique but since they appear as a flat background they cannot be misinterpreted as delayed emission.

As a numerical example we can consider an experiment where we detect 10^4 photons per second with a repetition rate of 1 MHz. On average, every one out of hundred laser pulses will be followed by a photon detection event meaning that the probability to detect two photons after one laser pulse is only 10^{-4}. This means that we will only discard only 0.01 % of all real photons while we discard roughly half of all the afterpulse events.

3.2 QD film charging experiments

3.2.1 QD synthesis

Materials
Lithium perchlorate (LiClO4, 99.99%), CdO (99.99%), Cd(II)-acetate (99.995%), Zn(II)-acetate (99.99%), Octadecene (ODE, 90%), 1,7-heptanediamine (7-DA, 98%), Oleylamine (OLAM, 99.8%), Oleic acid (OA, 90%), Ferrocene (Fc, 98%), Butanol (BuOH, Anhydrous, 99.8%), Methanol (MeOH, Anhydrous, 99.8%), Hexane (99.8%, Anhydrous), Octadecylphosphonic acid (ODPA, 97%), Trioctyl phosphineoxide (TOPO, technical grade, 90%), Trioctylphosphine (TOP, 97%), 1-Octanethiol (>98.5%), Selenium powder (Se, 99.99%), Tellurium powder (Te, 99.997%), and Acetonitril (99.99%, Anhydrous) were all bought from Sigma-Aldrich and used as received unless specifically mentioned below. Before usage, the acetonitril was dried in an Innovative Technology PureSolv Micro column.

Core synthesis
The CdSe core QDs were synthesized based on a method by Chen et al.[34] 60 mg of CdO, 280 mg of ODPA and 3 g of TOPO were mixed in a 50 mL three-neck flask. These solids were heated up to 150 °C under vacuum, the solids melted and the resulting liquid was kept at this temperature for 1 h to degass. Next, the liquid was heated to 320 °C, where it turned colorless and clear. After the solution became clear, 1 mL TOP was added and the temperature was increased to 380 °C. At this temperature, the Se-precursor (60 mg Se in 0.5 mL TOP) was injected quickly. After 25 s, where the QDs were allowed to grow, the reaction mixture was cooled by compressed air to room temperature. The product was washed twice by adding a 1:1 solution of methyl acetate and centrifugation at 3000 rpm. The precipitated QDs were redispersed in hexane. After washing, the QDs were filtered by a 0.2 mm millipore filter and stored in a nitrogren purged glovebox.

Shell Synthesis
Synthesis of Cd-oleate and Zn-oleate for CdS and ZnS shell growth.
To produce the Cd-oleate precursor, 1.32 g of Cd(II)-$(acetate)_2$ was mixed with 52.4 g ODE and 7.4 g of OA. The mixture was heated to 120 °C under vacuum for 3 hours. Finally, the mixture was cooled down and stored in a nitrogen purged gloveboxe.
The Zn-oleate precursor was made similarly by addition of Zn(II)-$(acetate)_2$ to 1 g of OA, 1.6 mL ODE and 1.6 mL of OLAM. The mixture was heated to 130 °C in a nitrogen purged glovebox.
Shell growth of CdS and ZnS.
The growth of CdS and ZnS shells around CdSe QDs were performed based on an adapted method by Chen et al.and Boldtet al.[16, 34]
First, growing of the CdS shells was done by mixing 20 nmol CdSe cores, 2.6 mL octadecene (ODE) and 0.6 mL degassed oleylamine (OLAM) to a 100 mL three neck flask. The mixture was degassed for one hour at room-temperature and for 20 hours at 120 °C. Next, the solution was slowly heated to 310 °C. When the temperature reached 240 °C, the Cd-oleate precursor and 1-octanethiol were injected dropwise to grow CdS shells at a rate of half a CdS monolayer per hour. After this, 1 mL of OA was quickly injected and the solution was kept at 310 °C for 1 h to allow annealing of the shells and core. Before

the ZnS shell growth, the solution was degassed for 1 h at 120 °C.
Next, ZnS shells were grown on the CdSe/CdS core/shell QDs. The CdSe/CdS QD solution was heated to 280 °C. When the solution reached 210 °C, Zn-oleate and 1-octanethiol in 4 mL ODE were separately injected to ensure a growth rate of 2 monolayers of ZnS per hour. After precursor addition, the solution was cooled by compressed air. The solution was washed twice by addition of methanol:butanol (1:2), centrifugation at 3000 rpm for 10 minutes and redispersion of the precipitate in hexane. Finally, the solution was filtered through millipore filters with a pore diameter of 0.2 mm and stored in a nitrogen purged glovebox.

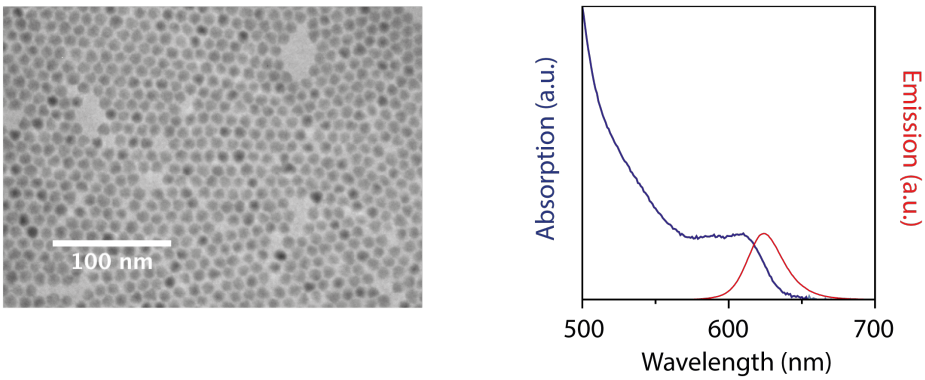

Figure 3.5: Characterisation of CdSe/CdS/ZnS core/shell QDs. TEM image of CdSe/6CdS/2ZnS core/shell QDs with an average size 8.5 ± 0.9 nm, obtained from a TEM image by averaging over 50 QDs. PL emission maximum is at 630 nm.

3.2.2 Electrochemical charging of QD films

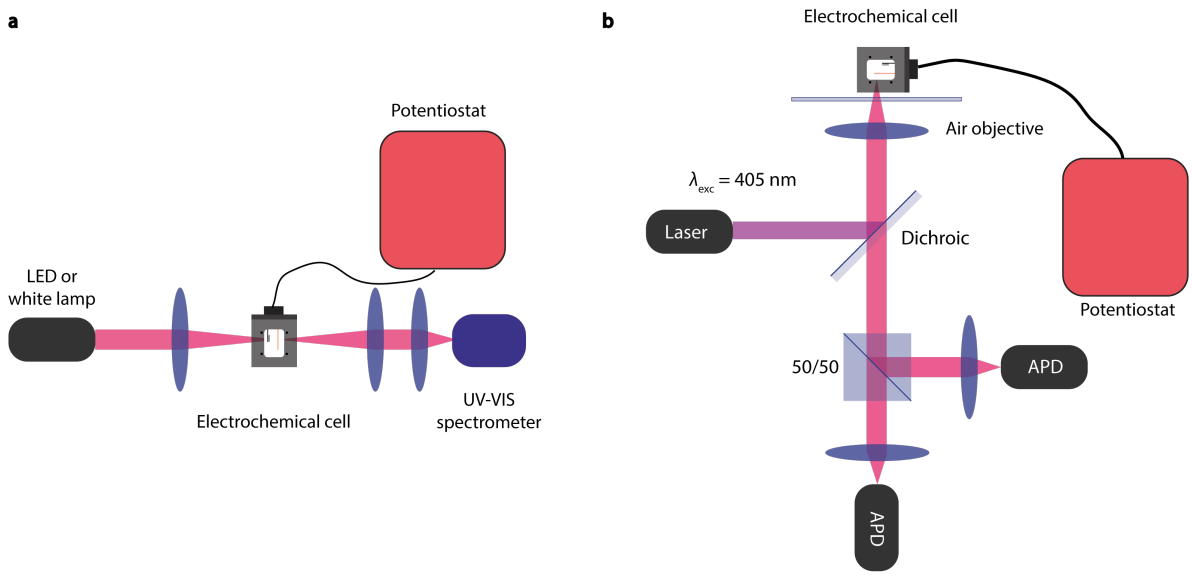

Figure 3.6: Schematic of QD charging setups (**a**) Setup inside nitrogen purged glovebox where a QD film on ITO is put inside an electrochemical cell. Absorption or emission spectra are measured as a function of potential by applying a voltage over the QD film while illuminating the sample either with a white lamp (absorption) or a LED (emission). (**b**) Same spectroscopic setup used for the single QD measurements except here we use a air objective with M=7.

QD film preparation

QD films were prepared by dropcasting a stock solution of CdSe/CdS/ZnS QDs in hexane on a slightly tilted Indium Tin Oxide (ITO) coated conductive substrate. After evaporation of the solvent, the film was treated with a 1,6-diaminohexane solution to crosslink the QDs, preventing the QD film to dissolve in the electrolyte. The film was washed with methanol to remove the excess 1,6-diaminoheptane.

Cyclic voltammetry in combination with absorption/emission spectra

Method adapted from [18]. The CdSe/CdS/ZnS films were loaded in a electrochemical cell filled with 0.1 M $LiClO_4$ in acetonitrile electrolyte together with a Ag wire reference electrode and a Pt counter electrode. The measurements were performed in a nitrogen purged glovebox. The voltage over the QD film was controlled by a PGSTAT128N Autolab potentiostat. Absorption and PL emission measurements as a function of potential were measured by a UV-VIS spectrometer USB2000 from Ocean Optics. The light was coupled in with a fiber. A cyclic voltammogram (CV) was recorded from the open circuit potential V = -0.2 V to -1.6 V and back three times with a scan rate of 20 mV/s. The potentials reported in this thesis are with respect to a Ag wire in electrolyte solution. The potential of the Ag electrode was calibrated by reference to a ferrocene/ferrocenium couple, from which the reduction potential is well known.

Cyclic voltammetry in combination with QD film decay dynamics

Cyclic voltammetry in combination with decay dynamics measurement are performed out-

side the glovebox, hence the electrochemical cell is prepared in the glovebox and made airtight to prevent oxygen from leaking in. Abundance of oxygen will be detrimental for charging of the QD film because of its redox activity. The same spectroscopy setup as was used for the single QD experiments will be used, except we use an air objective (Magnification $M \approx 7$) for excitation and emission collection.

Chapter 4

Decay dynamics of single QDs

Abstract **– Colloidal quantum dots (QDs) have exciting optical properties, which can be tuned by varying parameters like chemical composition or size. The excited state dynamics, responsible for these exciting properties, can be studied on the level of individual fluorescent QDs using decay dynamics measurements. Colloidal QDs show intermittency of the fluorescence between a bright and dim state on a single particle level, this peculiar intermittency phenomenon is called blinking. In the beginning of this chapter we will show the two main blinking models which show random switching of decay dynamics on a single QD level. Sometimes photon emission takes significantly longer. This phenomenon, called delayed emission, is commonly attributed to trap states that temporarily store charge carriers thereby delaying recombination. In the second part of this chapter we study delayed emission from single CdSe/CdS core/shell QDs. The results reveal that the possibility for temporary trapping of hot or cold charge carriers switches on and off seemingly randomly during an experiment of several minutes.**

4.1 Prompt emission of single QDs

4.1.1 Charged-state blinking

QDs show switching between a bright and a dim state randomly in time, also known as blinking.[7, 8] Much research was done, both theoretically [9] and experimentally [19, 35], to explain the microscopic origin of this phenomenon. Over the years two main blinking mechanisms found approval in the scientific community. The first mechanism explains blinking by random charging/discharging events and is referred to as Charged-state blinking.[19] The second mechanism explains blinking by allowing excitons to recombine non-radiatively via shallow trap states and is called Quantum yield blinking.[35] Interestingly, both blinking mechanisms are found experimentally, even within a same batch of quantum dots. This chapter will discuss both mechanisms elaborately and shows that by looking at prompt emission, e.g. photons resulting by direct recombination of an exciton, much can be learned about this peculiar phenomenon.

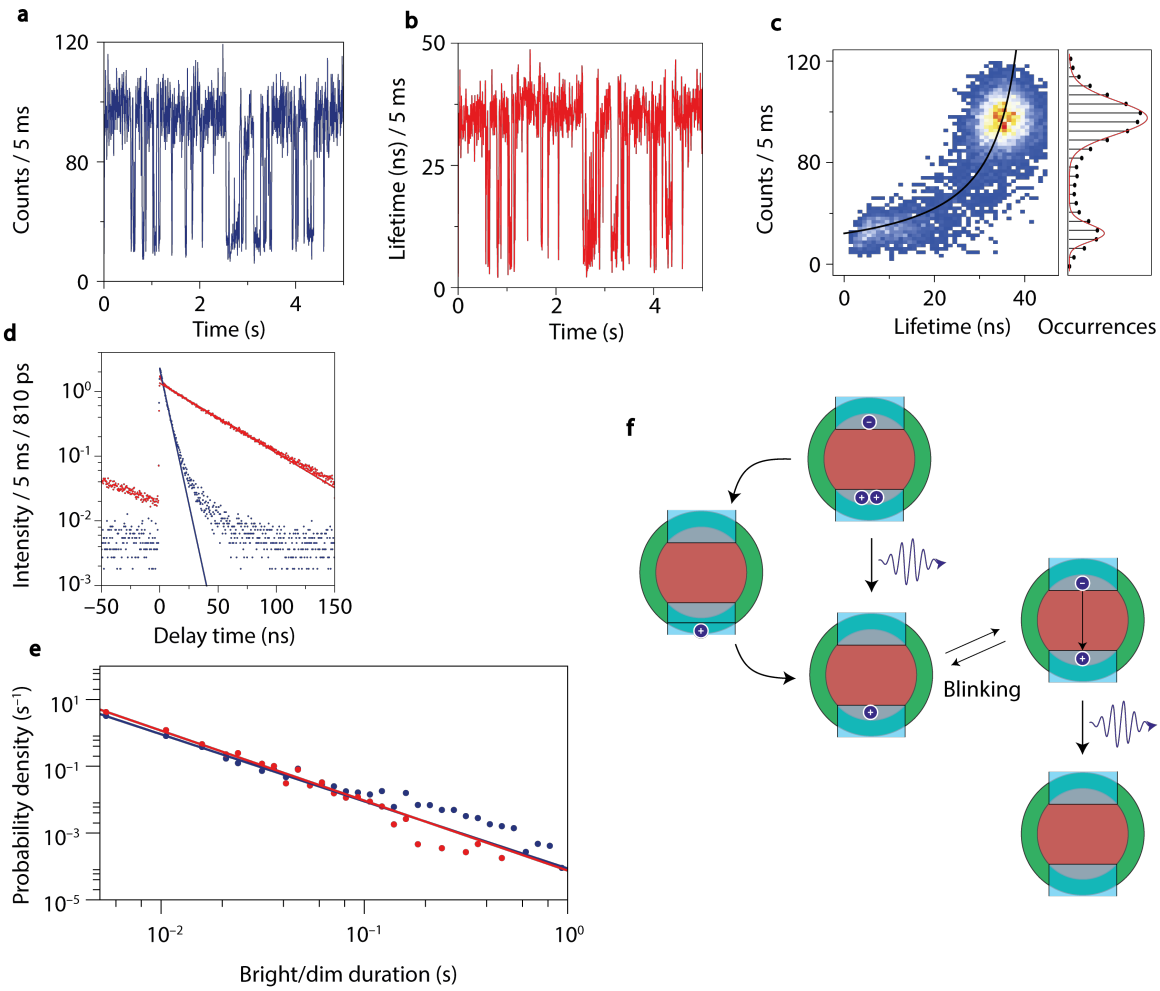

Figure 4.1: Charged-state blinking. **(a)** Intensity trace of a single CdSe/8CdS/2ZnS QD showing blinking between a bright state (100 photons / 5 ms) and a dim state (30 photons / 5 ms). (**b**) Average lifetime of all time intervals from (**a**), showing correlation between a long-lived bright state and a short-lived dim state. (**c**) Fluorescence Lifetime Intensity Distribution (FLID) to visualize the correlation between the intensity and the average lifetime of the QD, fast subsequent blinking events result in points between the two states. The black curve shows the mixing of these two states by fast blinking. (**d**) Decay curve of the bright(red) and dim (blue) state showing mono-exponential decay and a higher amplitude for the dim decay curve. This indicates that the dim state is a charged state. (**e**) A histogram of bright/dim durations on a double-logarithmic scale indicating a broad distribution of durations. (**f**) Mechanism of charged-state blinking where the QD blinks between a charged and an uncharged state.

Charged-state blinking was first proposed by Efros and Rosen in 1997.[8] They referred to the blinking behaviour as a random telegraph signal in close analogy to the random electronic switching in bulk semiconductor materials. Switching between a bright and dim state in this model is driven by charging/discharging events mediated by bi-exciton Auger recombination. Recombination of one of the two excitons will transfer its energy to one excited charge carrier thereby leaving the QD effectively charged.

Figure 4.1 (**a**) shows the intensity trace of a single CdSe/8CdS/2ZnS QD where the number of photons per 5 ms time interval are given for an experimental time of 4 s. The intensity trace shows switching between a bright state with intensity of 100 photons / 5 ms and a dim state with an intensity of 30 photons / 5 ms. The average photon arrival time can be calculated for all 5 ms time intervals. For single exponential decay this is equal to the lifetime of the excited state. Figure 4.1 (**b**) shows the average arrival time for the same experimental time as the intensity trace. A clear correlation between the number of photons and the average arrival time can be observed, the bright state has an average arrival time of 37 ns and the dim state has an average photon arrival time of 8 ns.

To visualize the correlation between the intensity and the average photon arrival time, we construct a Fluorescence Lifetime Intensity Distribution (FLID) in figure 4.1 (**c**), which is a 2D histogram with the intensity per 5 ms on the y-axis and lifetime on the x-axis. A histogram of the intensity per 5 ms shows the Poissonian noise giving rise to a Poisson distribution around the two mean values of the bright and dim state of the QD. The random blinking events can be almost completely resolved using a bin width of 5 ms. Faster subsequent blinking events however, result in an intensity and lifetime by a summation of the time spent in either state, given by

$$I = (1 - f)I_{\text{bright}} + fI_{\text{dim}}, \tag{4.1}$$

where I corresponds to the total intensity, f corresponds to the fraction of time the QD spends in the dim state and I_{bright} and I_{dim} are the intensities of the bright and dim state. Based on the lifetimes and intensities of the bright and charged state, the mixing of these two states can be reproduced [35] by the formula

$$\tau = \frac{I_{\text{bright}} I_{\text{dim}} (\tau_{\text{dim}} - \tau_{\text{bright}})}{I_{\text{bright}} - I_{\text{dim}}} \frac{1}{I} + \frac{I_{\text{bright}} \tau_{\text{bright}} - I_{\text{dim}} \tau_{\text{dim}}}{I_{\text{bright}} - I_{\text{dim}}}. \tag{4.2}$$

Based on the intensities and lifetimes of the bright and dim state, we can plot this formula in the FLID (black). This shows that the points in between the bright and dim state are merely due to fast blinking events, where the QD spent a fraction of the time in either state.

Figure 4.1 (**d**) shows the decay curve of the bright (red) and dim (black) state where selection is based on a threshold intensity of 70 photons/5 ms. The decay curve is normalized to the total amount of experimental time spent in the bright or dim state. We observe a long-lived bright state as expected with a lifetime of 37 ns and short-lived dim state with a lifetime of 8 ns. Interestingly, the amplitude of the decay curve is not equal for the bright and dim state. Assuming an equal absorption cross section for the bright and dim state, we would expect an equal average number of excitons formed per laser pulse. In the theoretical background it was explained that the amplitude of a decay curve is proportional to, $I(t = 0) \propto \gamma_{\text{r}} N(0)$. We therefore have to conclude that the radiative rate is approximately higher by a factor two in the dim state. This can be explained by an additional charge carrier present in the QD making the QD effectively charged. In the theoretical background we saw that a higher radiative rate in a charged QD can be explained by having twice the number recombination pathways compared to the uncharged case. In the experiment we actually obtain an amplitude ratio which has a value of 1.73, reflecting the deviations from the simplicity of statistical scaling. Including

Coulombic interactions between the two electrons in the 1S energy level will lower the value of the overlap integral between oppositely charged charge carriers. Therefore we can expect the radiative rate in the charged state to be smaller than twice the radiative rate of the bright state. We can however still estimate the Auger rate by assuming that statisticaling scaling holds. Based on a radiative rate γ_{r} of 1/37 ns^{-1} and a total rate γ_{X^-} of 1/8 ns^{-1} we obtain by using

$$\gamma_{\mathrm{X}^-} = 2\gamma_{\mathrm{r}} + 2\gamma_{\mathrm{A}}, \tag{4.3}$$

an Auger rate γ_{A} of 0.035 ns^{-1}.
To quantify the seemingly random switching behavior of a single QD between a bright and a charged state we can construct the distribution of bright/dim durations in the experiment. Based on the same threshold as was used for separating the two decay curves, we can now count all the durations of the QD spent in the bright or charged state. Figure 4.1 (**e**) shows a histogram of the bright durations (blue) and dim durations (red) on a double logarithmic scale. Both show an extremely broad distribution which can be fitted by a power-law function with α=2. This broad distribution of both the bright and dim durations indicates that there is not a single rate of going from the bright to the dim state and vice versa.
Figure 4.1 (**f**) shows the mechanism of charged-state blinking. On the bottom right the QD is in the ground state, excitation by a laser forms an exciton. This exciton can recombine thereby emitting a photon again. However, a charging or blinking event can drive the QD to a new meta-stable groundstate which is higher in energy. Next excitation event will generate an excited state with one electron in the $1S_e$ energy level and two holes in the $1S_h$ energy level. Now, the electron can recombine with two holes which results in non-radiative Auger processes where recombination of the exciton promotes the hole to a higher energy level. The hot hole can lose its energy to phonons quickly to give the meta-stable ground state again. Again a random discharging event can bring the QD back into the neutral optical cycle.

4.1.2 Quantum yield blinking

The previous section showed a blinking model where a QD switches between a charged and an uncharged state. Here, we will show a different mechanism of QD blinking also commonly encountered in colloidal QDs. Figure 4.2 (**a**) shows an intensity trace of a single CdSe/4CdS QD sample where the QD switches seemingly random between three different states. The bright state has an intensity of 120 photons/10 ms, the medium bright state has an intensity of 60 photons/10 ms and the dark state has an intensity of 5 photons/10 ms. Correlating the average lifetimes and the intensity in a FLID again shows three distinct states of the QD where the average lifetime decreaseses linearly with the intensity. A histogram of the intensities can be fitted well by a summation of three Poisson functions. This time two thresholds of 100 and 40 photons/10 ms is used to separate the medium bright state and the bright state from the dark state. Figure 4.2 (**c**) shows the normalized decay curves where the bright state (red) has a single exponential lifetime of 22 ns and the medium state has a single exponential lifetime of 12.5 ns. Comparison of the two decay curves shows that the amplitude is almost exactly the same

for the two states, indicating equal radiative rates which corresponds to the proposed QY blinking model. The decay curve of the dark state is given in black. Although the lifetime is significantly faster as expected for a state even more dim, the amplitude is also much smaller which cannot be explained by this QY blinking model.
We can again look at the distribution of bright and dim durations of the single QD. The threshold is set to 100 photons/10 ms, therefore we only look at the blinking events between the bright state and the medium/dark state combined. Figure 4.2 (**d**) shows again a broad distribution of both the medium/dark (red) and the bright (blue) durations. Both can be fit by a power-law function.Interestingly, while the different blinking models show completely different change in decay dynamics, the blinking behavior has the same characteristic broad distribution. What trap states result in Quantum yield blinking or Charge state blinking is still unclear.
Figure 4.2 (**e**) shows the mechanism of Quantum yield blinking where in the bright state excitons always recombine radiatively after formation of an exciton. Blinking events can drive the QD to dim state with a lower QY where radiative exciton recombination is in direct competition with non-radiative recombination via shallow trap states. This pathway does however not affect the radiative rate of the single QD unlike charged-state blinking.

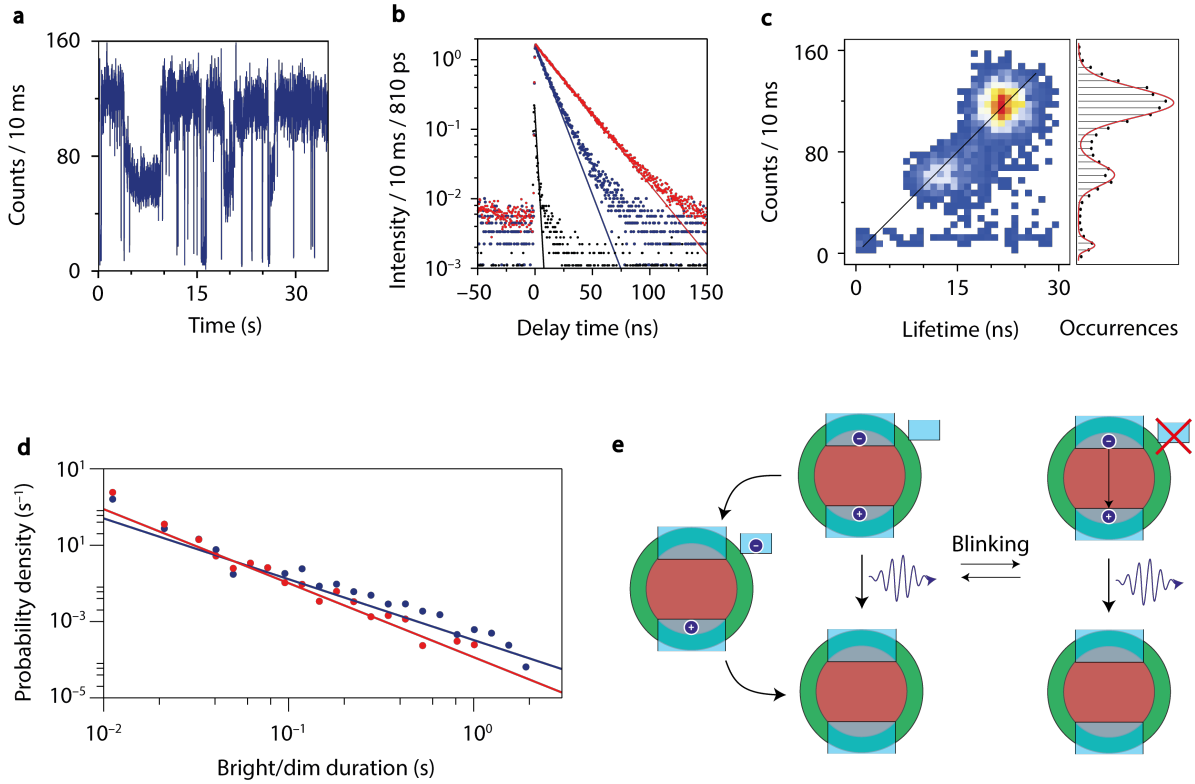

Figure 4.2: Quantum yield blinking. (**a**) Intensity trace of a single CdSe/4CdS QD showing blinking between three states with different intensity (bright state 120 photons / 10 ms, medium bright state 70 photons / 10 ms and dark state 5 photons / 10 ms). (**b**) The FLID shows correlation between the intensity and the average lifetime of the state, the intensity decreases linearly with lifetime. (**c**) Decay curve of the bright state (red) and the medium bright state (blue), separated from the dark state by two threshold values of 100 and 40 photons / 10 ms. Both decay curves have the same amplitude indicating equal radiative rates. (**e**) Mechanism of Quantum yield blinking where in the bright state the QD emits a photon after every excitation. Switching to a dim state opens a non-radiative shallow trap state which is in competition with radiative decay. Opening of this non-radiative pathway lowers the QY.

4.2 Delayed emission of single QDs

In an ever demanding society where both industry and civilization stride to 100 percent efficiencies, understanding processes of loss is extremely relevant. Mandkind tries on a large scale to avoid formation of heat in processes where this is not the relevant energy form, for example lights and chemical reactions. Here, we will show results on loss processes on one of the smallest scales possible. We will show on a single quantum dot level that excited charge carrier trapping, which is most frequently assumed to be a large loss mechanism in semiconductor industry, can actually be a reversible process where no energy is lost. By the use of decay dynamics measurements, employing resolutions down to the nanosecond, it was possible to shed light on the process of trapping. Two different mechanisms of excited charge carrier trapping are present. The first mechanism involves ultrafast trapping (sub-ps timescale) from a hot-carrier state and is therefore called hot-carrier trapping. The second mechanism, involves trapping on a much slower scale (ns). All charge carriers cooled down to the band edge before trapping and therefore this is called cold-carrier trapping. Peculiarly, while the trapping rates differ over 5 orders of magnitude, release of the charge carriers both in hot-carrier as in cold-carrier trapping occurs on the time scale of microseconds.

4.2.1 Decay dynamics characterisation of delayed emission

Here, we show the decay dynamics of delayed exciton recombination on single CdSe/CdS QDs (see method for sample characterisation). To be able to probe the decay dynamics at longer timescales than for example the prompt emission discussed in the previous chapter we use a lower repetition rate. This allows us to monitor the arrival of photons up to 1 μs after excitation, i.e. the typical timescale for the release of trapped charge carriers. Figure 4.3 (**a**) shows a decay curve of a single CdSe/CdS QD where in the first 100 ns the decay dynamics can be described by single exponential decay (red, single exponential fit). We attribute this single exponential decay to direct recombination of an exciton. For delay times larger than 100 ns, the decay dynamics start to deviate from single exponential and can be fit (green) by power law function. As was discussed in the theoretical background, this type of decay dynamics can be attributed to trapping and subsequent release of charge carriers. Recombination of the exciton after release of the charge carrier results in delayed exciton emission. Now, we will examine the emission of these delayed photons in experimental time to shed some light on the microscopic origin of trapping.
Figure 4.3 (**b**) shows the emission intensity trace of the same CdSe/CdS QD over a period of 40 seconds. The intensity trace shows similar blinking behaviour of the emission traces where analysis showed blinking between a neutral and a charged-state.
Since we want to extract information about excited state dynamics taking place at much longer timescales, we perform time-gating of emission photons. We discard all photons arriving the first 400 ns after the laser pulse because these mainly arise due to direct recombination of the exciton and therefore masks the release of trapped charge carriers. Fig 4.3 (**c**) shows the intensity trace where only photons arriving after 400 ns are counted in the same experimental time as figure 4.3 (**b**). Interestingly, seemingly random bursts of delayed photons are detected in time where the highest intensity per 10 ms is roughly

15 % of the total intensity. While the total intensity blinks between two different emission intensities, the delayed intensity does not seem to have a stable level of high or low delayed emission intensity. This could however simply be an artefact of the binning procedure, where the switching rate between the high emission intensity and low emission intensity is much faster than the 10 ms timescale of binning. A more elaborate analysis of this behaviour will follow in the next chapter.

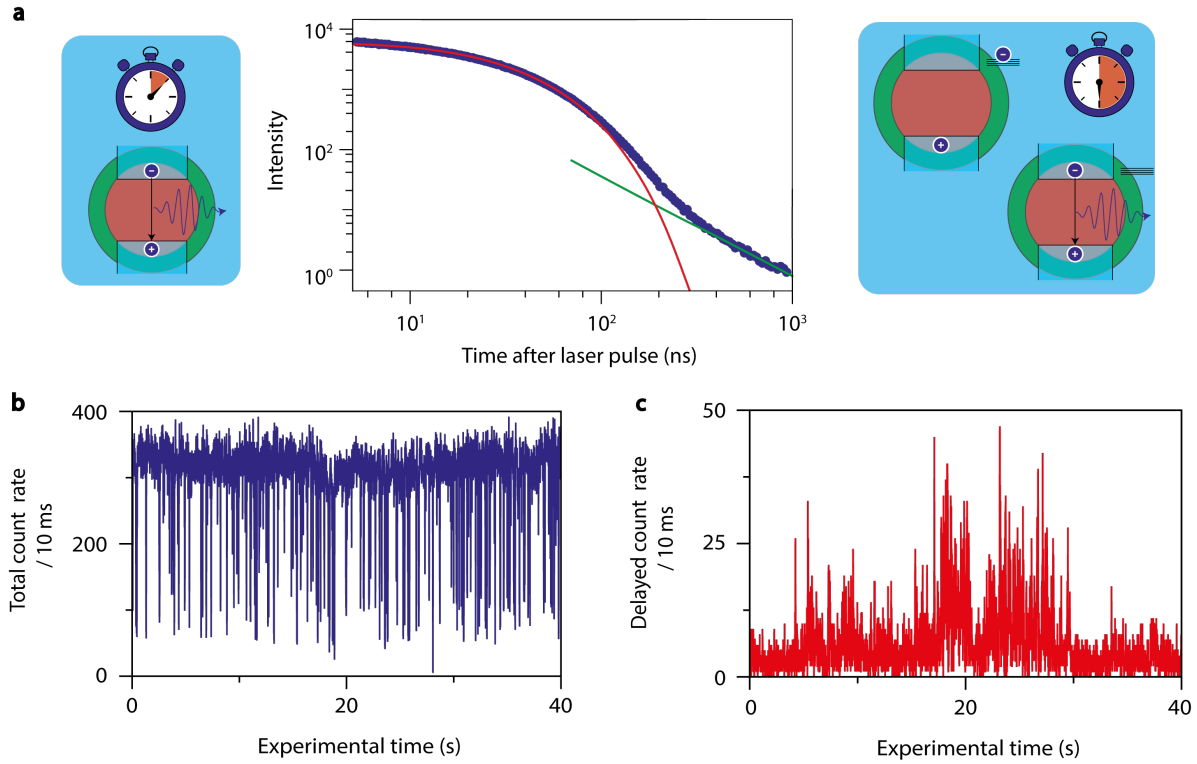

Figure 4.3: Decay curve and count rate of a single CdSe/CdS QD. (**a**) Decay curve of single QD where the 100 ns shows single exponential decay (red, single exponential fit) attributed to direct exciton recombination. For delay times longer than 100 ns the decay dynamics start to deviate from single exponential decay (green, power-law decay fit), this is attributed to delayed exciton emission where a charge carrier is trapped and released before recombination. (**b**) Intensity trace of a single QD where the QD blinks between two intensities. The bright state has a countrate of 320 photons/10 ms and the dim state, which was identified that be a charged state, has a countrate of 80 photons/10 ms. (**c**) Time-gating on the intensity trace, e.g. discarding photon detection events with a delay time smaller than 400 ns, shows bursts of delayed emission up to 40 photons/10 ms seemingly uncorrelated to the blinking behavior.

We characterise the short bursts of delayed intensity by a similar threshold analysis used in the previous section to separate the bright and dim state. Although here we do not have a clear splitting between a bright and a dim state, we can select all moments in time where we consider the delayed intensity to be high for a delayed countrate of > 10 photons/10 ms. We consider the delayed countrate to be low for < 5 photons/10 ms. We additionally only select moments in time when the total countrate is > 300 photons/10 ms. This last selection we do to make sure we are only looking at the bright state of the

QD, thereby not mixing decay dynamics of the bright and dim state.
Decay curves of these selected moments in experimental time are given in figure 4.4 (**a**) where we observe the high delayed intensity decay curve in red and the low delayed intensity decay curve in green. All decay curves and intensity traces are corrected for the effect of after pulsing, which could also give significant intensity compared to the delayed emission intensity as discussed in the method. The red decay curve shows, as expected, characteristic power-law decay at long delay times with a power-law exponent $\alpha = 3.0$, whereas the green decay curve only shows approximately single-exponential decay. Additionally, we observe a lower amplitude of the red decay curve showing delayed emission. This is characterised in figure 4.4 (**b**) where the ratio between the red and the green decay curve is given. The intensity ratio of 0.65 remains constant up to delay times of 10 ns, this indicates that the decay rate of prompt emission of the red and green decay curve are the same.
A proposed model which can explain the observations is shown in figure 4.4 (**c**). We propose a mechanism where hot charge carriers are trapped with a rate γ_{HT} before they can cool down to the conduction band edge with a rate γ_{c}. Opening of this trapping pathway is seemingly random in time giving rise to bursts of delayed intensity. When this hot-carrier pathway opened, we will have a lower population of the lowest-energy exciton state which results in a lower amplitude as we saw in the theoretical background. Additionally, the radiative decay to the groundstate is unaffected in this model, which we see in experiment by the constant ratio of the decay curves. A distribution of release rates followed by radiative decay from the lowest-energy exciton state will result in delayed emission. To be able to compete with charge carrier cooling, the trapping rate γ_{HT} must be of the same magnitude. Therefore, we can estimate the trapping rate to be on the order of 1/ps, which is the typical order of magnitude of hot electron cooling rate in CdSe/CdS QDs as reported by Rabouw et al. by pump-push-probe spectroscopy.[36]
A similar analysis was performed on 8 other single QD measurements (Appendix B) showing the same hot-carrier trapping mechanism contributing to delayed emission. Interestingly, CdSe cores also seem to show hot-carrier trapping as shown in 4 different single QD measurements in Appendix B. However, the intensity trace shows no blinking between a bright and dim state so threshold selection analysis is tedious. Therefore we do not draw hard conclusions from this.

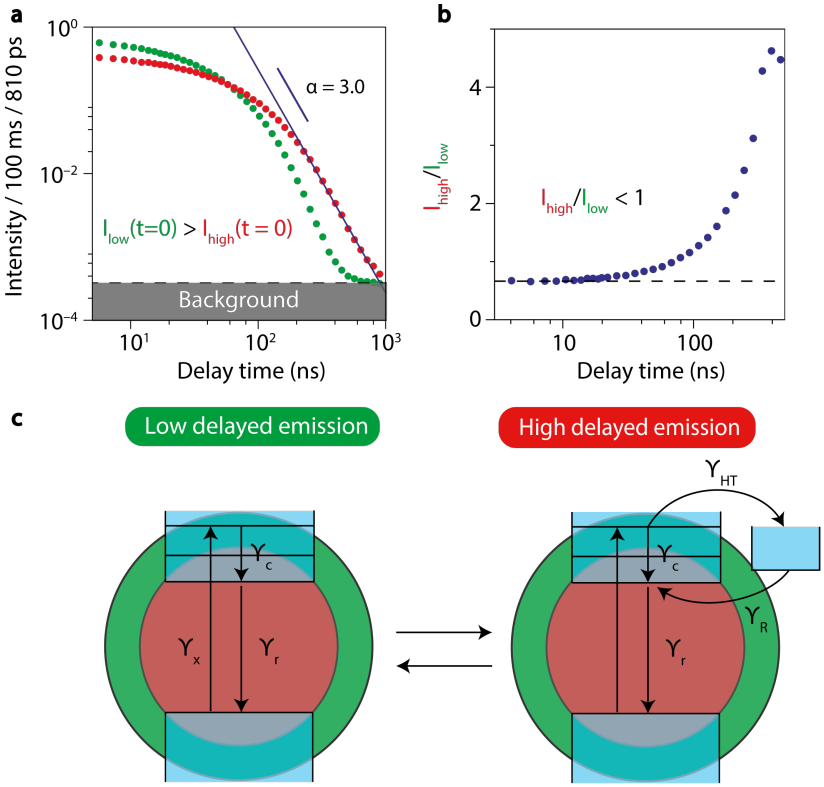

Figure 4.4: Hot-carrier trapping in single QDs. (**a**) Comparison of the red and green PL decay curves shows a difference in the amplitude. The amplitude of the PL decay curve when delayed emission is prominent is smaller. (**b**) Dividing the two decay curves shows a constant ratio of 0.65 indicating no infuence of delayed emission on the prompt emission lifetime. (**c**) A lower amplitude of the red decay curve can be interpreted as very fast trapping from a hot-carrier state in competition with hot-carrier cooling. This trapping does not change the lifetime of the QD but changes the population of excited charge carriers at the lowest-energy exciton state.

So far we reported 9 different single QD experiments all showing opening of a hot-carrier trapping pathway contributing to delayed emission. However, in one experiment we found a fundamentally different trapping process contributing to delayed emission. A similar threshold analysis distuingishing high and low delayed intensity for the bright state was performed. Figure 4.5 (**a**) shows the decay curves of high (red) and low (green) delayed intensity. Again, the red decay curve shows characteristic power-law decay with a power-law exponent α=1.6. The amplitude of the decay curve is exactly the same which means that the population of the lowest-energy exciton state is equal. We observe however that the green decay has a longer lifetime which means that the exciton decays slower. In figure 4.5 (**b**) the faster decay for the red decay curve is visualized by plotting the ratio of the two decay curves. An additional single exponential rate is present in the prompt emission of the red decay curve of 1/120 ns.
We propose a mechanism to explain these fundamentally different observations in figure 4.5 (**c**). In this model hot charge carriers are allowed to cool to the lowest-energy exciton state. From here, opening of a trapping pathway in time with a rate γ_{CT} results in trapping of cold charge carriers. Trapping of charge carriers is now in competition with

direct exciton recombination resulting in a larger decay rate, which we observe in the decay curves.

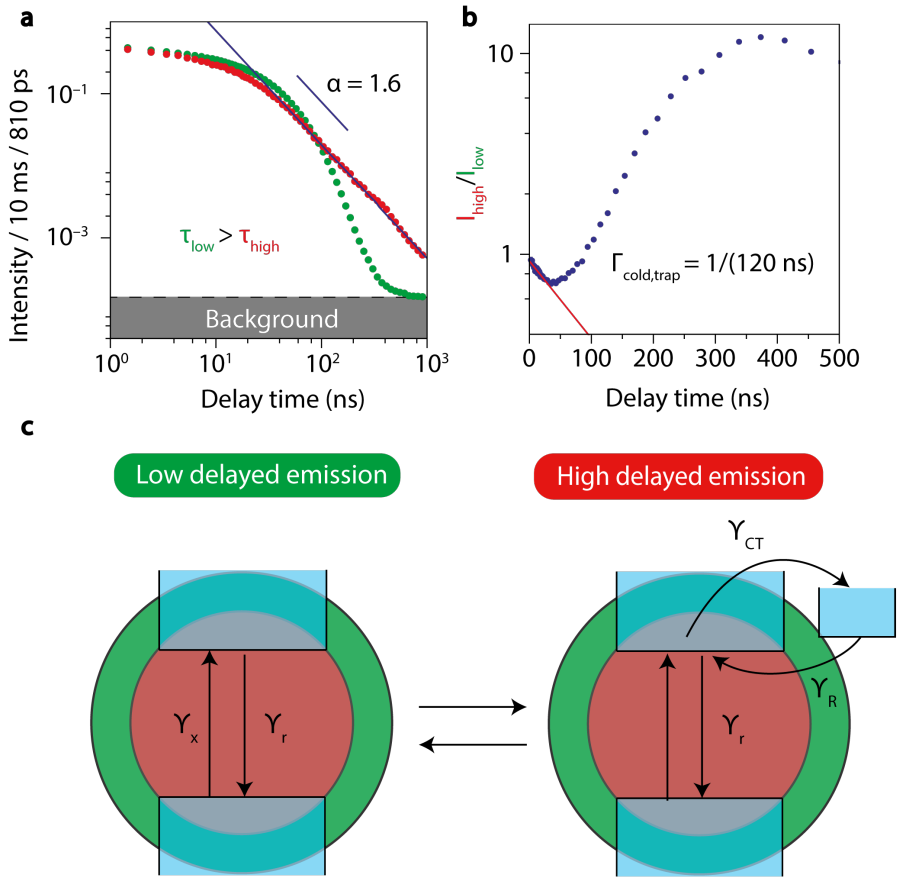

Figure 4.5: Cold-carrier trapping in single QDs. (**a**) Comparison of the red and green PL decay curves show a difference in the prompt emission lifetime. When delayed emission is prominent the prompt emission lifetime is shorter. (**b**) Dividing the decay curves shows addition of a single exponential rate of 1/(120 ns). (**c**) This additional rate can be interpreted as a trapping rate from the lowest-energy exciton state. Competition between radiative decay via direct exciton recombination and trapping results in a shorter prompt emission lifetime.

4.2.2 Timescale characterisation of delayed emission

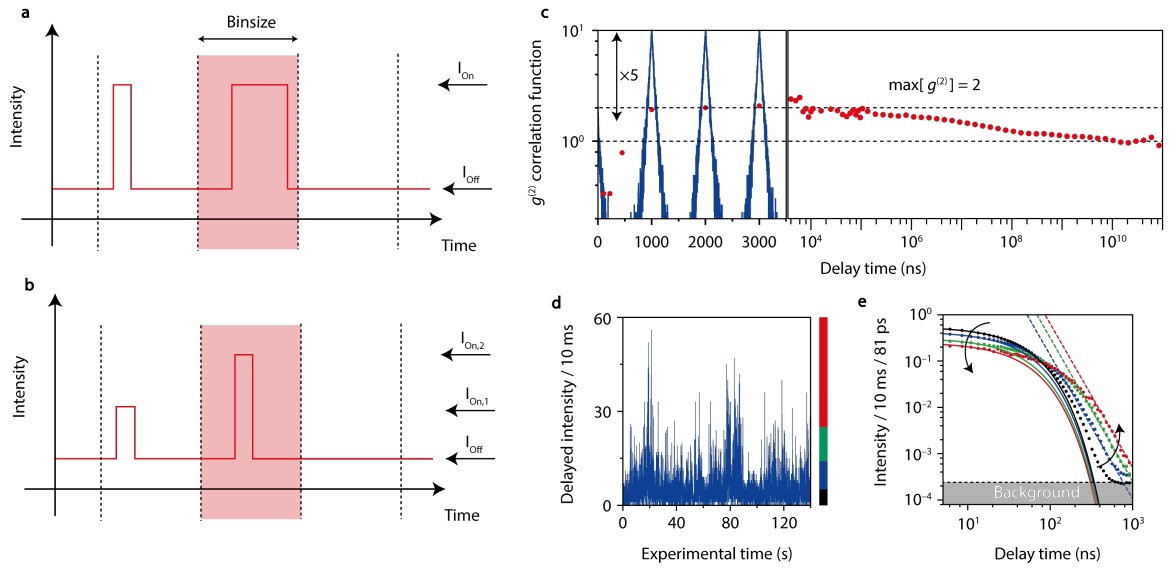

Figure 4.6: Photon statistics of delayed emission. (**a**) Model for delayed emission where the delayed intensity switches between an intensity I_{on} and I_{off} where the length of the bursts I_{on} can be different. (**b**) Model for delayed emission where the delayed intensity switches between several intensities but the length of the bursts stay the same. (**c**) Second order correlation function of time-gated (delay time ¿ 400 ns) single QD data. Logarithmic binning shows bunching up to approximately 1 ms, indicating an upper limit on the length of delayed emission bursts. (**d**) Delayed intensity trace where intensity axis is divided into segments. (**e**) Decay curves from the different segments showing a lower amplitude of the segments with a higher average delayed intensity. The release characteristics from the power-law decay stay the same, possibly indicating that the proposed model in (**a**) is valid.

In the methods chapter we showed that the second order correlation function obtained from a Hanbury Brown-Twiss experimental setup allows us to determine if we are collecting emission from a single emitter. Also, in the previous section we explained that assigning a time scale to blinking statistics is possible since switches between on and off are slow enough to resolve by a simple counting procedure. Here, we will use the second order correlation function to shed light on the typical timescales at which these bursts of delayed emission are present, where simple counting procedures fail due to fast switching.

Inspection of the delayed intensity trace in figure 4.4 (**b**) showed no blinking between two intensity levels like prompt emission. In principle, two scenarios can account for the bursts of delayed intensity. Either, figure 4.6 (**a**), every burst of delayed intensity has a different length but an equal intensity. In this picture, for every time interval the intensity is determined by the total amount of time the hot-carrier trapping pathway was open. The other scenario, 4.6 (**b**), is that the rate of hot charge carrier trapping changes over time but the length is constant.

We now assume scenario 1, where we can describe the bursts of delayed emission in time

as a linear superposition of a distinct state where delayed emission is high with an intensity I_{on} and a state where delayed emission is low with an intensity I_{off}. In this model, for a very high switching rate, every time interval in our experiment will consist of a fraction high delayed emission f and a fraction low delayed emission $1 - f$. With this assumption we can characterise the timescales of delayed emission by using the second order correlation function.
For a completely incoherent source of light we know that the intensity at some time $t+T$ is completely uncorrelated to the intensity at time t and therefore the second order correlation $g^{(2)}$ equals one. In this respect we would expect $g^{(2)}$ to go to one in the limit of infinite times in our experiment, since the QD has no memory in what state it was before. Because of anti-bunching of a single QD, $g^{(2)}$ goes to zero for zero time delays. Interestingly, for intermediate time differences, i.e. long compared to the time between laser pulses but short compared to memory loss, we can expect bunching because of fast switching behaviour. For delayed intensity switching we can describe the maximal value of $g^{(2)}$ in terms of the on and off intensities by

$$\max[g^{(2)}(\tau)] = \frac{I_{\text{on}} + I_{\text{off}}}{\langle I \rangle} - \frac{I_{\text{on}} I_{\text{off}}}{\langle I \rangle^2}, \tag{4.4}$$

where $\langle I \rangle$ is the average intensity. A derivation of this equation can be found in Appendix C. To check whether this rather simple model of fast switching between two states gives information about the timescales of delayed emission, we plot the second order correlation function $g^{(2)}$ of a single QD experiment. We use time-gating, e.g. discarding photon detection events with a delay time ¿ 400 ns, to probe the timescales of delayed emission. Figure 4.6 (**c**) shows $g^{(2)}$ for the single QD measurement showing hot-carrier trapping as the responsible mechanism for delayed emission. The left part of the graph shows the usual $g^{(2)}$ correlation function for pulsed excitation at a linear time scale with anti-bunching at zero delay times. For longer timescales we plot the correlation function on a logarithmic timescale till 100 seconds time delay. From this graph we can see that indeed there is bunching, $\max[g^{(2)}] = 2$. For delay times $g^{(2)}$ longer than 1 ms $g^{(2)}$ starts to decrease to one. We attribute this time of 1 ms as the typical timescale at which delayed emission turns off. From $g^{(2)}$ on large time scale we can also see that the bunching spans several orders of magnitude in time. This indicates that scenario 2 for delayed emission is unlikely, since this would show as a narrow peak in $g^{(2)}$.
With the obtained maximum of $g^{(2)}$ together with the delayed emission intensity trace we can reproduce the intensity of delayed photons when the hot-carrier trapping pathway is opened I_{on}. To compute this, we need the average intensity of delayed photons and we need to obtain the intensity of delayed photons when hot carrier trapping is negligible, i.e. I_{off}. Figure 4.6 (**d**) shows again the delayed emission trace of a single QD over time from where we determine the average intensity $\langle I \rangle = 5.6$ photons/10 ms. Based on an estimated for $I_{\text{off}} = 5$ photons/10 ms we can now determine I_{on} by using the equation given above. The intensity of the on state $I_{\text{on}} = 58$ photons/10 ms. Therefore it seems that some bursts have a duration of 10 ms since we see intensities close to 60 photons/10 ms in our experiment.
Another experimental check whether one (4.6 (**a**)) or multiple (4.6 (**b**)) delayed intensity levels are present for a single QD can be obtained by looking at the delayed emission dynamics as a function of delayed intensity. Figure 4.6 (**d**) shows four vertically subdivided

segments of the delayed intensity trace. For each of these segments, the accumulated decay curve is plotted in figure 4.6 (**e**) in the corresponding colour. As expected, the amplitude of the decay curve decreases with increasing delayed intensity and the power-law decay increases with increasing delayed intensity. Interestingly, the power law exponent α does not change as a function of the delayed intensity as indicated by the power law fits depicted by the dashed lines. This indicates that the distribution of release rates stays approximately the same. In the model where the QD switches between multiple intensity levels, it is unlikely that every intensity level has exactly the same release dynamics. Therefore, the model from figure 4.6 (**a**) is more likely to explain bursts of delayed emission but we cannot entirely rule out scenario 2.
In conclusion, the model where a single QD switches very fast between emitting a large amount of delayed emission photons and emitting almost zero delayed emission photons seems to work fairly well. Using the second order correlation function allows us to analyse the characteristic timescales of burst of delayed photons, ranging from 1 μs to 1 ms. Subdividing the delayed emission trace in segments of increasing delayed intensity also verifies that selecting time intervals with more delayed photons simply gives us a higher fraction of the time the QD could trap hot charge carriers.

4.2.3 Spectral characterisation of delayed emission

Thus far we have characterised delayed recombination of charge carriers in single CdSe/CdS quantum dots observing the PL decay dynamics and the second order correlation function. We have stated already that ultrafast trapping at the picosecond scale traps either a hot electron or a hole, after which we assume that the trapped charge carrier is released again and recombines with the remaining charge carrier (see figure 4.7 (**a**)). In this section we will investigate if single QDs actually show release of trapped charge carriers which results in exciton recombination or that perhaps trap state emission takes place (see figure 4.7 (**b**)). To verify this, we will simultaneously measure the decay dynamics and the spectrum of a single QD.

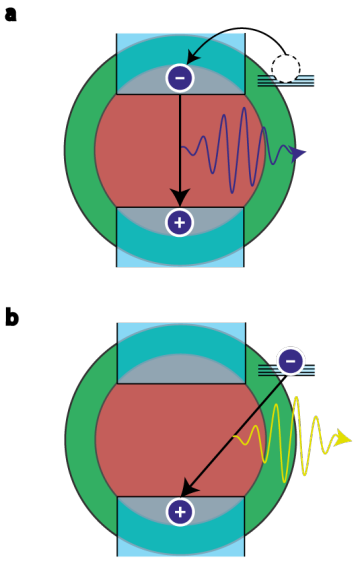

Figure 4.7: Delayed emission or trap state emission. (**a**) Trapped charge carriers are release to the lowest-energy exciton from which exciton recombination results in photon emission. (**b**) Recombination of a trapped charge carrier is called trap state emission and results in emission of photons with a different energy.

A typical delayed intensity trace is depicted in figure 4.8 (**a**) where bursts of delayed intensity are observed to about 80 photons/50 ms. If we select the time intervals where the delayed intensity is high we observe again a decay curve, figure (**b**) red, with a lower amplitude with respect to the decay curve with low delayed intensity green. This ensures that we are measuring a single QD where hot-carrier trapping is contributing to delayed emission.
Now we do not only know how many delayed photons are emitted per unit time, but also what the spectrum of the single QD was within that same experimental time. Figure 4.8 (**c**) shows the integrated spectra for moments in time where the QD emitted many photons (total photons > 600/50 ms) but few delayed photons (red, < 24 photons/50 ms) and the integrated spectra where the QD emitted many photons and also many delayed photons (black, > 25 photons/ 50 ms), normalized to the total integration time. We see that actually the spectrum of high delayed intensity is significantly more red as compared to low delayed intensity (low delayed emission $\lambda = 633$ nm, high delayed emission $\lambda = 641$ nm).

At this point we might argue that photon emission is slow only because the wave function overlap between a trapped charge carrier and the remaining charge carrier is lower. A paper by Baker et al. showed that it is possible to introduce redshifted trap state emission by the introduction of additional mercaptopropionic acid ligands and a paper by Rabouw et al. Time Resolved Emission Spectra (TRES) showed that CdSe nanoplatelets showed significant redshifted trap state emission of delayed photons.[26, 20] However, these papers show that trap state emission is something that occurs when normal exciton recombination is also present. Now, we will try to elucidate which mechanism, release and recombination or trap state emission, contributes to delayed exciton emission.

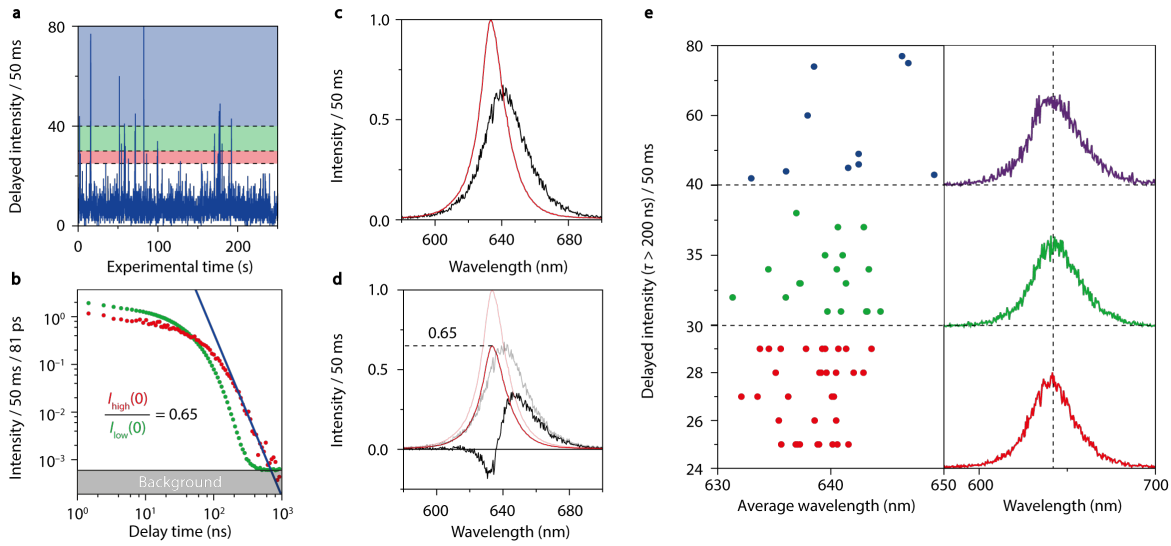

Figure 4.8: Spectral and decay dynamics of single QDs. ((**a**) Delayed intensity trace of a single QD, divided into three segments.(**b**) Comparison of high and low delayed emission shows hot-carrier trapping contributing to delayed emission. (**c**) Spectrum of a single QD when the delayed intensity is low (red) and when delayed intensity is high (black), the delayed emission spectrum is slightly broader and a little bit red-detuned from the low delayed intensity spectrum. (**d**) If the observed delayed emission spectrum would be a summation of direct exciton emission and trap state emission we should be able to reconstruct the trap state emission by subtraction of 65 % of the low delayed intensity spectrum. Subtraction shows that the intensity falls well below zero indicating that both exciton and delayed emission is redshifted during delayed emission. **e**) Spectra from the segments selected in (**a**) on the right show no change of shape with increasing average delayed intensity. Additionally no clear correlation between the delayed intensity and the average wavelength per time interval is observed. This is again experimental evidence in favour of both exciton and delayed emission being broader and red-detuned when hot-carrier trapping pathways are open.

As a first check we will subdivide the delayed emission trace in segments of increasing delayed intensity, see figure 4.8 (**a**). If the integrated delayed emission spectrum is merely a summation of exciton emission and relatively red trap state emission, we would expect that the segments with a higher mean delayed intensity must be significantly more red. On the left side of figure 4.8 (**b**) the average wavelength per time interval is plotted as a function of delayed intensity. From these average values of single spectra recorded in 50 ms there is no clear increase of the average wavelength as a function of delayed intensity. On the right of this figure the accumulated spectra for the different segments are plotted. Here, no clear difference is present between the segment where a moderate amount of delayed intensity ($25 \leq N < 30$) is present and the segment where a high delayed intensity ($40 \leq N < 80$) is present. The spectrum at high delayed intensity is broader than the moderate delayed intensity spectrum. This could be due to the relatively short total integration time of this spectrum of only 500 ms.
We can also try to reconstruct the delayed emission spectrum assuming that delayed emission is trap state emission. In the theoretical background it was explained that the amplitude of a decay curve is proportional to the population of the lowest-energy exciton state. For this particular experiment we know that the amplitude of the decay with high delayed intensity is 0.65 times the amplitude of the decay curve with low delayed intensity. If we assume that the delayed emission spectrum is a summation of direct exciton recombination and trap state emission, we should be able to get the trap state emission spectrum by subtracing 65 % of the spectrum of low delayed intensity from figure 4.8 (**c**). Figure 4.8 (**d**) shows the result of this computation, a significant part of the spectrum drops below zero, even up to 36 % of the original maximal value. From this, in combination with the unchanged spectrum as a function of the delayed intensity, we conclude that the delayed emission spectrum does not result from trap-state emission. Interestingly however, both direct exciton emission and delayed emission have a broader spectrum and is redshifted when hot-carrier trapping pathways are open.

Chapter 5

Spectroelectrochemistry of QD films

Abstract **–Colloidal quantum dots (QDs) have exciting optical properties, which can be tuned by varying parameters like chemical composition or size. The excited state dynamics, responsible for these exciting properties, can be studied by systematically varying the emitting state of the QDs. In this part, a CdSe/CdS/ZnS film in electrical contact with ITO will be subjected to a decreasing voltage. Decreasing the voltage moves the Fermi level towards the bottom of the conduction band and electrons will be injected in the doubly degenerate 1S energy level. Observing the decay dynamics at more negative voltages shows a gradual shift from neutral excitons (X^0) to a combination of neutral, singly (X^-) and doubly (X^{2-}) charged excitons, which can be modelled by Fermi Dirac statistics. Additionally, observing the delayed emission as a function of voltage shows that the delayed intensity scales with the fraction of neutral QDs. This can be explained either by a model where injection of electrons into trap states is kinetically hindered or by a model where no electrochemical trap state filling is possible but the probability for double charge carrier trapping is negligible.**

5.1 Prompt emission of QD films vs. applied voltage

In this section we will show how the decay dynamics of CdSe/6CdS/2ZnS QDs (absorption/emission spectra and TEM images shown in methods chapter) changes as a function of applied voltage. Figure 5.1 (**a**) shows the position of the Fermi level at zero applied voltage, which is exactly in the middle between the conduction and the valence band. At this voltage we have negligible occupation of the conduction band by electrons. As the voltage becomes more negative, the Fermi level will be shifted upwards to the bottom of the conduction band.[37] When the applied voltage roughly equals the value of the 1S energy level, e.g. $V{=}{-}V_{1S}$, electrons are injected into this enery level. We expect to observe a bleach of the 1S absorption since a part of the 1S energy levels is already occupied. Further decreasing the voltage, e.g. $V < -V_{1S}$, will eventually completely fill the doubly degenerate 1S energy level and the transition will be completely bleached.
Fig 5.1 (**b**) shows a cyclic voltammetry (CV) measurement on the QD film where the applied voltage is scanned from $V{=}{-}0.2$ V to $V{=}{-}1.6$ V and back three times with a

scan rate of 20 mV/s. Reversible bleach and regeneration of the 1S absorption at 612 nm is observed. Additionally, bleaching of a second peak at 470 nm is present, which is due to decreased absorption of the CdS shell. The absorption bleach is normalized to the maximum absorption bleach of the CdS shell. As discussed in the theoretical background, additional electrons in the QD will lower the QY by introducing non-radiative Auger processes. Simultaneous measurement on the emission of the QDs as a function of the potential (figure 5.1 (**c**)) shows that the PL intensity indeed drops as a function of voltage. Figure 5.1 (**d**) shows a 1D trace of the fractional absorption bleach fractional PL intensity as a function of the applied voltage obtained by fitting a Gaussian function at every potential.

We observe a strong increase in the absorption bleach of the 1S transition while simultaneously the PL quenches around a potential of $-1.3V$. If we assume that a complete bleach of the 1S transition corresponds to injection of two electrons per QD we can calculate the average number of electrons injected $\langle N \rangle$ in the QD by using $\langle N \rangle = -2\Delta A/A_0$. From this we can see in figure 5.1 (**d**) that we indeed inject 2 electrons per QD since the 1S absorption is completely bleached at V=−1.5 V. We must state at this point that this is a simplified version of the truth. We see from the CV absorption measurement that the 1S and the CdS absorption bleach at the same time. Therefore, we have to conclude that when the 1S absorption is bleached completely we have injected at least two electrons per QD.

So far, we observed a complete absorption bleach of the 1S transition and simultaneous quenching of the PL luminescence by decreasing the voltage. These observations are in line with the statistical scaling model introduced in the theoretical background where injection of electrons should bleach the 1S transition by electron injection and quench the PL by introducing Auger processes. Now, we will show results on the decay dynamics of the QD film as a function of the applied voltage. Decay dynamics will provide information not only on $\langle N \rangle$, but als the distribution of the number of injected electrons. We expect by inspection of the absorption bleach as a function of voltage a gradual increase of the number of injected electrons. Before we show the results, we will first try to derive a model from first principles which might explain the gradual shift from neutral (X^0), singly charged (X^-) and doubly charged (X^{2-}) excitons as a function of applied voltage. Let's assume we can describe the QD film as a number of QDs which can exchange heat and electrons with a reservoir at constant temperature T and constant chemical potential μ. In this picture we can use the grand canonical partition function to predict the probability that a single QD will accept zero, one or two electrons from the reservoir. Since we are probing so many QDs simultaneously, this probability for a QD accepting a number of particles from the reservoir will naturally convert to the fraction of QDs that accepted a number of particles. We will start by calculating the grand canonical partition function which has the general form,

$$\mathcal{Z} = \sum_i g_i \mathrm{e}^{\beta(N_i\mu - E_i)} \tag{5.1}$$

where we sum over all microstates where N_i particles have an energy E_i in contact with a heat reservoir where $\beta = 1/k_\mathrm{b}T$ and g_i is the number of microstates with the same

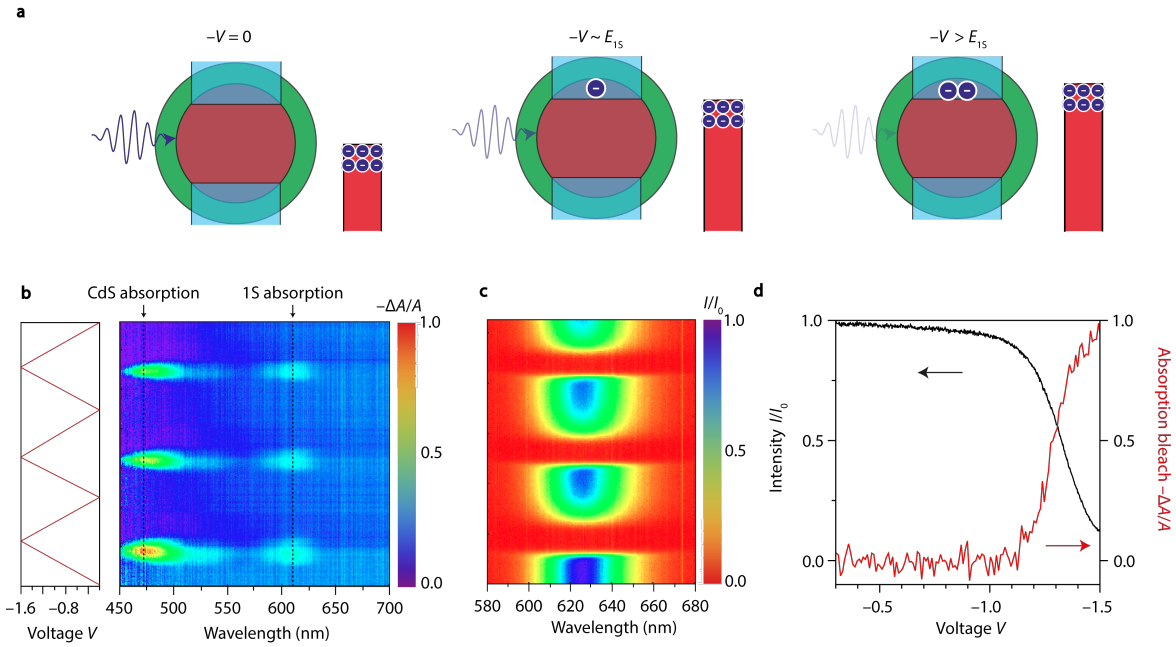

Figure 5.1: Absorption bleach and PL quenching of a QD film. (**a**) At the open-circuit potential the Fermi level is located exactly in between the conduction band and the valence band. Decreasing the applied voltage will shift the Fermi level upwards to the conduction band. When the applied voltage equals the V_{1S} energy level we start to inject electrons into this energy level and we expect a bleach of the 1S absorption. Further increase of the applied voltage will inject even more electrons into this energy level until the doubly degenerate 1S level is completely filled and the absorption is completely bleached. (**b**) A CV measurement on a CdSe/6CdS/2ZnS QD film where we scan from −0.2 V to −1.6 V and back three times with a scan rate of 20 mV/s shows that the CdS shell 470 nm and the CdSe 1S absorption 612 nm bleach and regenerate reversibly. (**c**) Simultaneous measurement on PL intensity shows that addition of electrons in the 1S energy level also quenches the emission by non-radiative Auger processes. (**d**) A 1D trace of both the fractional PL intensity and fractional bleach of the 1S absorption shows that around −1.3 V the PL drops and the absorption bleach increases significantly. If we assume that a complete bleach of the 1S absorption corresponds to injection of 2 electrons per QD, we can relate the fractional absorption bleach of the 1S absorption to the average amount of electrons injected per QD.

energy E_i. In our experimental setup we change the voltage to achieve a change in the chemical potential. Therefore, we apply the conversion $V = \mu/e$. We also convert the energy of state i to a potential difference, e.g. $E_i = eV_i$. The grand canonical partition function in terms of potentials is

$$\mathcal{Z} = \sum_i g_i \mathrm{e}^{\beta e(N_i V - V_i)} \tag{5.2}$$

The first microstate is a neutral quantum dot G^0, where zero electrons are injected $N_0 = 0$ and we set the energy of this microstate to zero, e.g. $V_0 = 0$. The second microstate corresponds to a singly charged QD G^-, where $N_1 = 1$ and $V_1 = V_{1\mathrm{S}}$, e.g. the potential of the 1S electron level. Since we can fill either state from the doubly degenerate 1S level with one electron, the multiplicity of this microstate is 2. The last microstate X^{2-} completely fills the 1S level with 2 electrons, so $N_2 = 2$ and $V_2 = 2V_{1\mathrm{S}}$. We can expect that the presence of two electrons in this energy level introduces electrostatic repulsions. Therefore, filling of the second level will cost an additional energy. We parametrize this additional energy by V_C turning the total energy of this microstate into $V_2 = 2V_{1\mathrm{S}} + V_\mathrm{C}$. We obtain for the partition function of the doubly degenerate 1S level

$$\mathcal{Z} = 1 + 2\mathrm{e}^{\beta e(V - V_{1\mathrm{S}})} + \mathrm{e}^{\beta e(2V - 2V_{1\mathrm{S}} - V_C)} \tag{5.3}$$

We can now calculate the fraction of neutral f_0, charged f_1 and doubly charged f_2 QDs as a function of applied voltage using

$$f_i = \frac{1}{\mathcal{Z}} g_i \mathrm{e}^{\beta e(N_i V - V_i)}. \tag{5.4}$$

By using the previously defined factor we end up with

$$\begin{aligned} f_0 &= \frac{1}{\mathcal{Z}} \\ f_1 &= \frac{1}{\mathcal{Z}} 2\mathrm{e}^{\beta e(V - V_{1\mathrm{S}})} \\ f_2 &= \frac{1}{\mathcal{Z}} \mathrm{e}^{\beta e(2V - 2V_{1\mathrm{S}} - V_C)} \end{aligned} \tag{5.5}$$

Now we can try to use this model to understand the change in decay dynamics as a function of the voltage. We measure decay curves as a function of voltage starting at the open circuit potential $V_\mathrm{OC} = -0.2$ V and decrease the voltage with steps of 0.1 V until -1.0 V after which we decrease the voltage in smaller steps of 0.05 V to have more data points on the voltage range where we observed a large variation in the PL and absorption bleach in the CV measurements. We assume in our decay dynamics experiments that we are in equilibrium, meaning that the average number of electrons per QD is fixed.
Figure 5.2 (**b**) shows three selected decay curves from the experiment at $V = -0.2$ V, -1.2 V and -1.3 V. We performed a CV measurement on the QD film before the PL decay measurements to make sure electron injection was possible. The initial CV measurement is also used to correct for an additional quenching of the PL intensity during the PL decay measurements. We ascribe this additional quenching to deposition of acetonitrile vapour on the glass which lowers the collection efficiency.

We see from the decay curves that as a function of the voltage the decay dynamics of the QDs become faster and the amplitude increases. This can be qualitatively explained by the statistical scaling model introduced in the theoretical background.[19] We saw that injection of electrons in the 1S energy level increases the radiative rate for singly X^- and doubly X^{2-} charged excitons, thereby increasing the amplitude. Secondly, injection of electrons introduces non-radiative Auger processes which increase the decay rate and lowers the QY of the QDs.
We can fit the decay curves by assuming the decay dynamics is determined by a distribution of neutral, charged and doubly charged excitons as depicted in figure 5.1 (**a**). A global least squares fitting procedure is used to fit all decay curves simultaneously with three amplitudes per decay curve and three constant total decay rates, describing the decay rate of the neutral, singly charged and doubly charged excitons. Figure 5.1 (**b**) shows the result of this fitting procedure (solid lines) for the decay curves at $V = -0.2$ V, -1.2V and -1.3 V, where we observe that this model fits the data well. Assuming statistical scaling of the amplitudes allows us to compute the fraction of neutral, singly and doubly charged excitons for the three decay curves which are given as insets in figure 5.1 (**b**). Already at the open circuit potential a significant amount ($f_1 = 30$ %) of singly charged QDs is present. This is unexpected since we expect all QDs to be neutral at the open circuit potential. We ascribe this to the initial CV measurement before the start of the experiment to check if electron injection is possible. We thereby injected electrons into the film, that we hoped would come back out when we turned off the voltage. However, slow movement of electrons out of the QD film resulted in a significant amount of singly charged QDs at the start of the decay dynamics measurement.
The fitted lifetimes of the neutral excitons is 20.7 ns, of the singly charged excitons 5 ns and the doubly charged excitons 1.5 ns. We would expect that based on the statistical scaling model we could determine the radiative rate and non-radiative Auger rate, but solving this system of linear equations gives unphysical negative radiative rates. Perhaps the changes of the radiative and non-radiative rates as a function of voltage cannot be explained by this simple statistical scaling model. We can expect deviations from this statistical model because of two arguments. Firstly, the assumption that the radiative rate scales with the number of possible recombinations is not entirely correct when considering coulombic interactions. Coulombic repulsions between the two electrons in the 1S state will effectively reduce the overlap integral between the electron and the hole. Therefore we expect the radiative rate of a charged exciton to be somewhat smaller than twice the radiative rate of a neutral exciton. This effect will have an even larger influence on the radiative rate of the doubly charged excitons. One of the electrons must be in an energy level with P type symmetry, which has an even lower overlap integral with a S type symmetry wave function. Secondly, we expect deviations of the non-radiative rates based on a similar argument. Auger recombination of electron and hole with equal wave function symmetry (1Se-1Sh) or different wave function symmetry (1Pe-1Sh) will have a different Auger rate. Unfortunately, without assuming statistical scaling we cannot determine the radiative rate or the non-radiative Auger rate.

Figure 5.2 (**c**) shows the fitted fraction of the QDs of the QD film in the neutral, singly charged and doubly charged state as a function of applied voltage. The fraction of neutral, singly charged and doubly charged QDs is modelled by the probability functions derived above based on the grand canonical partition function. The dashed lines show

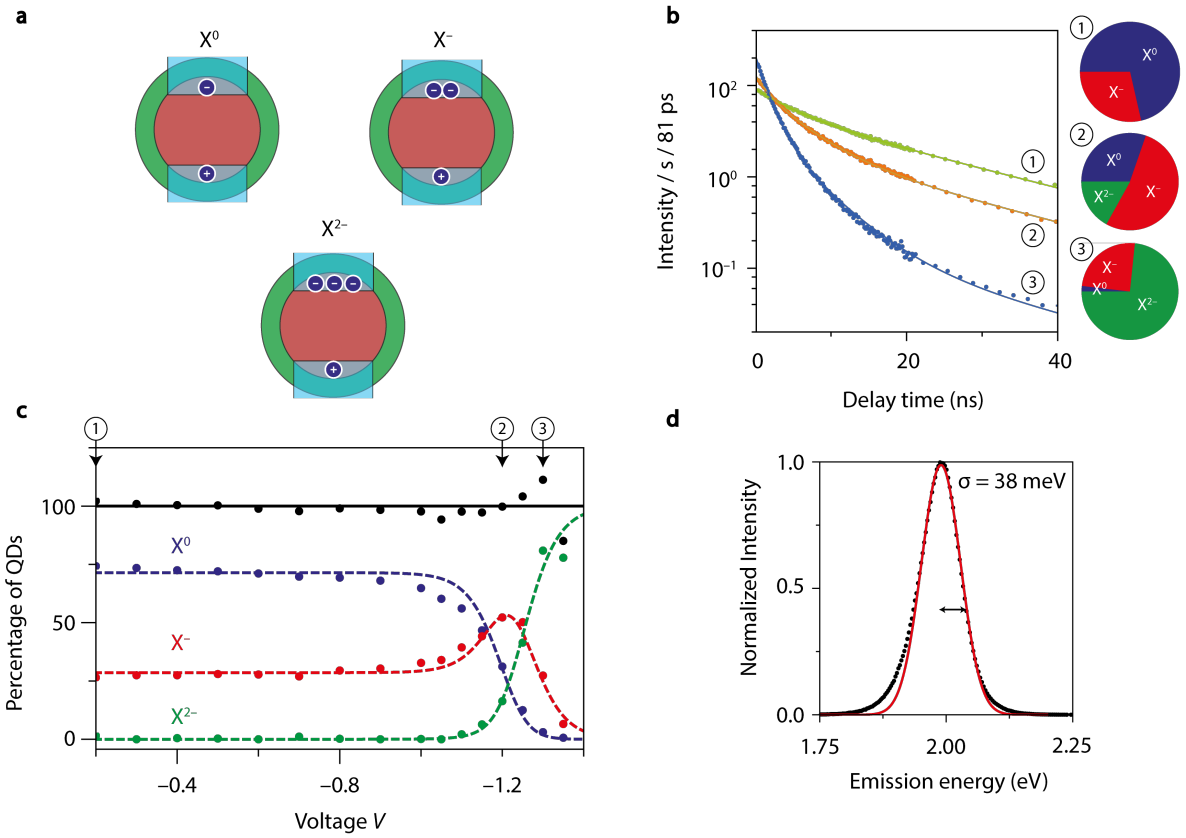

Figure 5.2: Decay dynamics as a function of applied voltage. (**a**) In the global fitting procedure, the possible emissive states of the QD can be neutral X^0, charged X^- or doubly charged X^{2-}. (**b**) Three PL decay curves at (1) $V = -0.2$ V, (2) $V = -1.2$ V and (3) $V = -1.3$ V. The decay curves are fit with a global fitting procedure with three fixed total decay rates and three different amplitudes per decay curve. The percentage of QDs in each state is given as an inset. The amplitude and total decay rate of the decay curve increases with applied voltage as expected from statistical scaling. (**c**) Fraction of neutral, charged and doubly charged QDs as a function of applied voltage obtained from a global fitting procedure. The dashed lines show the modelled fractions, starting with 70 % neutral QDs and 30 % charged QDs using the parameters $V_{1S} = -1.23$ V, $\beta = 40$ meV, $V_C = 2.5$ mV. (**d**) Standard deviation of a Gaussian fit of the PL data shows great similarity with the model parameter β indicating similar broadening mechanisms.

great resemblance with the fitted fractions assuming 70 % neutral QDs and 30 % singly charged QDs at the beginning of the experiment.
Based on this model we obtain an average potential of the 1S energy level of $V_{1S} = -1.23$ V. We determined this value by using this Fermi-Dirac model in combination with the PL decay measurements.
We obtain from this model a thermal energy of $k_b T/e = 40$ meV. We might have expected a thermal energy of $k_b T/e = 25$ meV, because these measurements were performed at room temperature. The apparent temperature is higher because of additional broadening mechanisms like a distribution of 1S energy levels and phonon coupling. The value of $k_b T/e$ determined from the Fermi-Dirac model is really close to the width of the PL spectrum obtained from the QDs in solution ($\sigma = 38$ meV) as can be seen in figure 5.2 (**d**). This indicates that the same broadening mechanisms responsible for the width of the PL spectrum are also contributing to the effective thermal energy of our experimental setup.
Lastly we determine a Coulombic repulsive potential of $V_C = 2.5$ mV for injection of a second electron to the 1S energy level. We can calculate the Coulombic energy of two 1S electronic wave functions spherically confined by the QD in first order by calculating $E_C = \langle\, 1Se1Se|V|1Se1Se \,\rangle$ where V is the electrostatic interactions between two charges separated by a distance r. Assuming the first particle-in-a-box wave function for both charge carriers the Coulombic energy is given by, $E_C = -1.79e^2/(4\pi\epsilon\epsilon_0 a)$, where a is the radius of the QD ($a = 5$ nm) and ϵ the dielectric constant of the QD ($\epsilon = 10$ for CdSe). The Coulombic energy has a value of 51 meV. This is unexpected since we obtain only a Coulombic energy of $E_C = 2.5$ meV. We can explain our experimental results by considering that the Li-ions in the electrolyte solution screen the excess charge carriers injected in the QD really well, e.g. approximately 5 % of the calculated charging energy remains.
A critical remark about the results is the fact that a relatively high amplitude of fast decay was present at the beginning of the experiment. We ascribed this to the presence of 30 % charged QDs due to an initial CV measurement. Unfortunately, the experimental setup did not allow us to verify the presence of 30 % singly charged QDs by a simultaneous absorption bleach of 15 %. In principle, the fast decay with a lifetime of 5 ns can also be explained by QDs having filled trap states below the conduction band. The filled trap state decrease the lifetime of the QDs by trap-assisted Auger recombination as was also seen in $CuInS_2$ nanocrystals by van der Stam et al.[18] This trap-assisted recombination will leave the radiative rate unchanged, which means that this decay comes from 60 % of the QDs instead of 30 %.
In conclusion, Fermi-Dirac statistics seems to provide a good description for how electron injection progresses as a function of the applied voltage. The statistical scaling of the radiative rates also works well to predict the fraction of QDs injected with zero, one or two electrons. The parameters on which this model is based can be reasoned on the basis of similar parameters obtained from the line broadening of the PL spectrum for the thermal energy $k_b T$ and charge screening of Coulombic repulsions by Li-ions leaving approximately 5% of the unscreened charging energy.

5.2 Delayed emission of QD films vs. applied voltage

In the previous chapter we showed that it is possible to electrochemically fill the doubly degenerate 1S energy level of CdSe/CdS/ZnS core/shell QDs. We also know from chapter 3 that hot-carrier trapping, where a hot charge carrier is trapped to a localized trap state, is the main mechanism responsible for delayed emission in single QDs. A logical next step in characterising these trap states is investigating if we can fill these trap states electrochemically, thereby possibly quenching delayed emission.

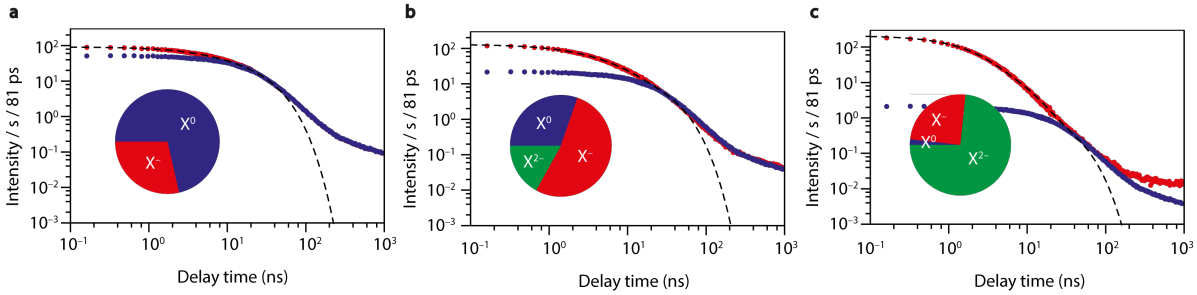

Figure 5.3: Delayed emission as a function of applied voltage (**a**) Decay curve of the QD film (red) on a double logarithmic scale at the open circuit potential $V = -0.2$ V, we assume that all delayed emission comes from the neutral QDs. The corrected decay without faster charged quantum decay is plotted in blue and the dashed line shows the global prompt emission fit. (**b**) Decreasing the voltage to $V = -1.2$ V shows increase of charged and doubly charged quantum dots as discussed in the previous section. Additionally, the delayed emission amplitude decreases proportional to the fraction of neutral QDs. (**c**) Further decrease to $V = -1.3$ V shows further decrease of the delayed emission amplitude proportional to the amount of neutral QDs. Deviation of the decay curve $V = -1.3$ V from the scaled neutral QD curve at high delay times is due to a relatively higher background because the QY decreased.

Figure 5.3 (**a**) shows decay curves on a double logarithmic scale at three different potentials, $V = -0.2$ V, $V = -1.2$ V and $V = -1.3$ V. We see that together with the prompt emission dynamics (delay time 0 – 100 ns) changing as described in the previous section (dashed lines show global triple-exponential fits), the delayed emission (delay time > 100 ns) intensity is simultaneously quenched. We observe that the delayed emission decreases as the fraction of neutral QDs decreases.
To quantify whether charged QDs show delayed emission, we make the assumption that 100 % of the delayed emission comes from neutral QDs. From the global fitting procedure, we determined $f_2 = 30$ % of the QDs were singly charged at the open circuit potential. If we want to test the hypothesis that the delayed emission scales with the amount of QDs that are neutral, we have to subtract the prompt emission dynamics from this singly charged population of QDs at the open circuit potential, e.g.

$$I_{\text{delayed}}(t, V = \text{V}_{\text{OC}}) = I_{\text{total}}(t, V = \text{V}_{\text{OC}}) - I_{f_2}(t, V = \text{V}_{\text{OC}}). \tag{5.6}$$

The corrected decay curve including only the prompt emission from the neutral QDs and 100 % of the delayed emission is plotted in 5.3 (**a**) at the open circuit potential. For

more negative potentials, this purely neutral QD decay is scaled with the fitted fraction of neutral QDs, e.g.

$$I_{\text{total}}(t,V) = I_{f_2}(t,V) + I_{f_3}(t,V) + A_{f_1}(V)\frac{I_{\text{delayed}}(t, V = \text{V}_{\text{OC}})}{I_{\text{delayed}}(t = 0, V = \text{V}_{\text{OC}})}. \tag{5.7}$$

The results of this is plotted in figure 5.3 (**b**) $V = -1.2$ V and (**c**) $V = -1.3$ V. We can see that the quenching of the delayed emission scales exactly with the amount of neutral QDs so the assumption of no delayed emission from charged quantum dots seems to match the data.
From this observation we can conclude that no trap states of QDs in the film are filled before the Fermi level reaches the bottom of the conduction band. If trap states are filled before injection of electrons into the 1S energy level, we would expect a decrease of the delayed intensity before changes in the decay dynamics. Another conclusion we can draw is that singly and doubly charged QDs apparently contribute a negligible amount to delayed exciton emission. We will try to estimate an upper limit of delayed emission from the singly charged QDs. To do this we apply again a global fitting procedure where we try to fit the delayed emission characteristics as a function of potential by a power law function, $A_{\text{del}}(V)t^{-\alpha}$, where the delayed emission amplitude as a function of potential is given by $xA_{X_0}(V) + yA_{X_-}(V)$, e.g. a fraction due to neutral QDs $x/(x+y)$ and a fraction due to singly charged QDs $y/(x+y)$. First we fit a power law function to the decay curve at the open circuit potential to obtain the power law exponent α. The amplitudes obtained from the prompt emission global fits are used to obtain an upper limit of the fraction of the delayed emission that comes from the singly charged QDs. From the global fit based on potentials $V = -0.2$ – -1.25 V we estimate that indeed nearly all the delayed intensity originates from neutral QDs. Delayed emission quenching is described by $x = 223.6$ and $y = 7.3 \times 10^{-15}$. Therefore, we conclude that we do not need delayed emission from the singly charged QDs to account for the delayed emission scaling.

Let's discuss the first conclusion. In case of trap filling before reaching the conduction band we expect quenching of delayed emission prior to a decrease in the fraction of neutral QDs. Therefore we conclude that trap state filling did not occur in this experiment before the Fermi level reached the 1S energy level. However, this does not automatically mean that there are no trap states that lie in energy below the 1S energy level. Filling of the trap states can be kinetically hindered at the timescales we measure in our experiment. Typically, after setting the potentiostat to a certain potential a net current will flow to reach this potential. After a while this net current is almost zero and the PL decay measurement is started. However, this net current in practice never becomes exactly zero. This could either be because of a current leak, e.g. redox active species or an actual leak in the potentiostat, or it could indicate that the QD film is not yet at its thermodynamic energy minimum and that trap states are filled extremely slow.
That trap state filling is extremely slow compared to the timescales of our experiment can be understood quite well in terms of movement of electrons in the film. When the potential is below the 1S potential, the population of free electrons in 1S states is low as determined by the Fermi-Dirac model. Injection of electrons via ITO tunnel from QD to QD to reach every trap state in every QD in the film. We consider that filling of trap states can either be mediated by hopping via 1S states or by direct via trap states.

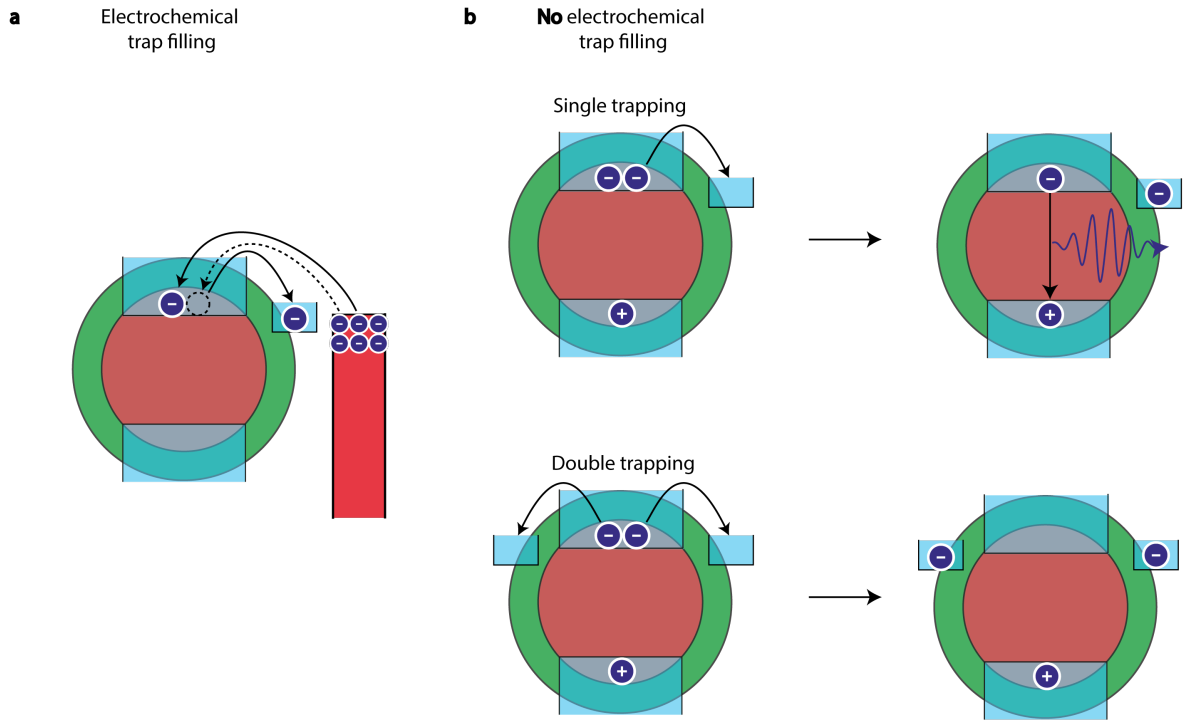

Figure 5.4: Mechanism delayed emission quenching. (**a**) Kinetically hindered filling of trap states could explain the onset of delayed emission quenching with electrochemical charging. Upon reaching the 1S energy level, all trap states are quickly filled via the 1S energy level. (**b**) Delayed emission quenching can also be explained by an argument where not electrochemical trap filling occurs at all. Injection of an electron in the 1S energy level yield the charged state. Single trapping of an electron will not result in delayed emission since regular neutral QD emission can take place. For delayed emission to occur for charged QDs both electrons must trap. Release of one of the two charge carriers results in delayed emission. Experimentally, it could be that the probability of double trapping is negligible and therefore delayed emission quenches proportional to the amount of neutral QDs.

Considering the fact that the film thickness is around several hundred nanometres, many tunnelling steps need to occur before trap states of QDs far away from the ITO are filled. Additionally, on average the distance between highly localized trap state wave functions will be larger than the distance between two 1S wave functions of neighbouring QDs. This will kinetically hinder trap state filling since the tunnelling probability scales exponentially with distance as we saw in the tunneling model for delayed emission in the theoretical background. Little is known about the distribution of trap state levels as a function of energy, but assuming a broad distribution of energies will hinder tunnelling even more since only a fraction of trap states is available for tunnelling at a certain applied potential. Therefore, we might argue that filling of the trap states is mediated by delocalisation of electrons throughout the QD film by hopping through 1S energy levels. The second observation from the delayed emission quenching is that apparently injection of additional electrons into the 1S energy levels prevents delayed exciton emission. From the first observation of delayed emission quenching which scales with the fraction of neutral QDs we proposed a mechanism where trap state filling is mediated by filling of the 1S energy levels. The distribution of 1S energy levels as a function of energy is determined by the polydispersity in size of the QD sample ($\approx$ 10 % for this sample). Typically, this distribution is fairly small, meaning that upon reaching of the bottom of the 1S level by tuning the Fermi level filling of the 1S goes relatively fast. Since the wave function of the 1S for type Quasi-type 2 QDs is delocalized in the QD, tunnelling between QDs becomes more likely and also filling of trap states that lie thermodynamically below the 1S energy level becomes highly probable. In this picture, simultaneous filling of all accessible trap states occurs instantaneously when the 1S energy level is filled. Here, we will explore if the presence of one (X^-) or two (X^{2-}) additional electrons in the emissive state can also alter the delayed emission characteristics without electrochemical filling of trap states. We will discuss how delayed emission from the singly charged QDs actually looks and maybe we can reason why the delayed exciton emission from this population is unlikely.

Figure 5.4 (**b**) shows the case where we have a singly charged QD with 2 electrons in the 1Se level and one hole in the 1Sh level. In the case of trapping from the band edge, one excess electron can be trapped from the 1S energy level. Subsequent release of the trapped charge carrier after several hundreds of nanoseconds could in principle result in delayed exciton emission. However, if we compare singly charged and neutral QDs, there is a big difference in the lowest-energy exciton state. After charge carrier trapping in neutral QDs, no emissive state is present since the hole that is left behind cannot recombine with an oppositely charged charge carrier. In the singly charged QDs on the other hand, trapping of only one of the excess charge carriers leaves behind an emissive state. Effectively, the singly charged QD can (and probably will) emit radiatively like a neutral QD before the trapped charge carrier can be released again. A little more quantitatively, the probability that a QD in the excited state, having a lifetime of 20 ns, will relax to the ground state within 100 ns is 99.3 %.

To get a non-emissive state in a charged QD, we need to have trapping of both 1S electrons. Trapping of both charge carriers from the 1S energy level will result in the same non-emissive state after trapping as for neutral QDs. Release of one charge carrier will result in delayed emission just like a neutral QD. If we assume that all delayed emission from the decay curve at the open circuit potential is from the neutral QDs,

we can calculate the trapping probability $P_S = 18.7$ %. Based on this single trapping probability, we can calculate the expected probability of detecting delayed emission from a double trapping event for singly charged QDs. For this, we assume that the QY of the neutral QDs is 100 %, $\gamma_t/(\gamma_t + \gamma_r) = 0.18$ and $\gamma_t + \gamma_r = 1/20$ ns, where γ_t is the trapping rate and γ_r is the radiative rate. Based on this system of equations we can estimate the trapping rate γ_t and γ_r and use this to calculate the probability for double trapping. The probability for double trapping from a singly charged exciton would be

$$\mathrm{P}_2 = \frac{\gamma_t}{\gamma_t + 2\gamma_r + 2\gamma_A} \frac{\gamma_t}{\gamma_t + \gamma_r} \tag{5.8}$$

where the first term describes the first trapping event where non-radiative processes are possible. The second term is the probability of the second trapping event (e.g. without the additional Auger rate). Based on a lifetime of singly charged QDs of 5 ns (obtained in the previous section) we estimate a probability of double trapping events of 0.77 %. However, we determined experimentally that the delayed emission from charged QDs is $\ll 0.77$ %. We can therefore argue that either the probability of double trapping is much smaller than we calculated based on these simple statistical arguments or there is simply not more than one trapping site, responsible for delayed emission, available per QD. The suggestion of simply having one trapping site is supported by similar research by Utterback et al. where they showed that delayed emission characteristics of CdS non-uniform nanorods can be fitted by a diffusion-like model (see theory) assuming approximately one electron trap state per nanorod.[22] Assuming hot-carrier trapping being the dominant mechanism for delayed exciton emission is even more restricting to have delayed emission from the singly charged state. Electrochemically inserted electrons cannot trap and therefore will always recombine before release of the other charge carrier.

In the context of material science, characterising trap states responsible for losses via non-radiative processes or reversible trapping processes like delayed emission in this case are extremely relevant. At this point, two different possibilities have been explained which both can explain the quenching of delayed emission when the Fermi level reaches the bottom of the conduction band. With an additional experiment, distinction between actual electrochemical trap filling or quenching of delayed emission by higher order trapping mechanisms can become clear. We propose an experiment where we cycle several times to potential values above the 1S energy level and below the 1S energy level. In this experiment the fraction of neutral QDs will decrease for more negative potentials and will increase again when the potential drops below the 1S energy level. The two different explanations will give a qualitatively different outcome of this experiment. If trap state filling is kinetically hindered, we expect to observe a lower delayed intensity after scanning the potential in the conduction band. We expect this because kinetic hindering of filling of a trap state below the conduction band will result in the same energy barrier to release the trapped electron. The release of trapped electrons will be kinetically hindered via an Arrhenius like expression where the release rate is proportional to $-\Delta E$, where ΔE is the energy difference between the 1S energy level and the trap state energy. The other possible outcome of the experiment is that we exactly predict the delayed emission intensity based on the amount of neutral QDs in the film. If this is the case probably the argument of a negligible probability of double and triple trapping holds and electrochemical trap state filling did not happen in these experiments.

Chapter 6

General conclusions and outlook

6.1 Conclusions

In chapter 4 we showed both characterisation of prompt emission and delayed emission of single CdSe/CdS QDs. In the first part of chapter 4 we experimentally verified that single QDs can blink via two different mechanisms. The first is charged-state blinking where the QD randomly switches between a dim charged-state and a bright neutral state and the second is quantum-yield blinking where the dim state has a lower QY due to shallow trap states in competition with radiative decay.
In the second part of chapter 4 we observed delayed emission of single CdSe/CdS QDs. We showed that two mechanisms can contribute to charge carrier trapping. The first is charge carrier trapping from a hot electron state which is in competition with hot electron cooling. The second one involves trapping on the ns timescale from the band-edge which is in direct competition with radiative decay. We characterised delayed emission due to hot-carrier trapping by employing the second order correlation function. We found that opening of the hot-carrier trapping pathway opens in time with a characteristic timescale of 1 ms. By looking at the decay dynamics in combination with spectral information we found that opening of the hot-carrier traps influence both the prompt emission as well as the delayed emission, showing a slightly broader and redshifted spectrum.

In chapter 5 we showed results on the electrochemical control over both the prompt and the delayed emission. In the first part of chapter we analyzed the prompt emission dynamics by modelling the decay dynamics with a model based on Fermi-Dirac statistics. Exploiting the Fermi-Dirac model, we showed in the second part of chapter 5 that quenching of delayed emission by tuning the Fermi level towards the conduction band is proportional to the fraction of neutral QDs in the QD film. We discussed the possibility of trap filling being mediated by the 1S energy level to explain this. An alternative explanation is also given where delayed emission is simply negligible for charged QDs because the probability of two subsequent trapping events is negligible.

6.2 Outlook

In this thesis different loss mechanisms were shown on the scale of individual QDs and of QD films. In the beginning of chapter 4 we saw non-reversible losses in the prompt emission due to unwanted Auger processes, driving QDs to dim charged states where they can optically cycle in up to several hundreds of milliseconds. In the next chapter we showed two different trapping mechanisms which can have a very different timescale of trapping (ps or ns scale), but both trapping mechanisms show release of the stored charge carriers within a few microseconds. Both blinking and delayed emission bursts are observed in a single QD at the same time at the ms timescale. It is unlikely to assume that these processes, which we can probe the dynamics of in 12 orders of magnitude in time (ps - s), are not related. Future experiments need to shed light on these peculiar set of timescales and here some possibilities for future research are given.
First, since both trapping responsible for blinking (Auger process promoting charge carrier to trap state) and trapping responsible for delayed emission (hot-carrier or cold-carrier trapping with subsequent release), it would be interesting to drive single QDs in a charged state for longer times and see how this influences the delayed emission characteristics. The electrochemical charging experiment in chapter 5 showed quenching of delayed emission proportional to the fraction of neutral QDs. Charging experiments on a single QD with simultaneous observation of delayed emission characteristics will be more convincing.
An experiment to further test our experimental finding of hot-carrier cooling being the dominant process responsible for delayed exciton recombination can also been done. By using a white-light laser, starting off at relatively blue excitation energy with respect to the QD bandgap, it must be possible to influence the delayed emission by detuning the laser to more red wavelengths. That is, before we are at the right energy for resonant excitation. Performing this experiment on a single QD would be convincing, since obviously not much is known about inhomogeneitys between single QD trap states in a QD sample.

Chapter 7

Acknowledgements

Ik wil in mijn dankwoord graag beginnen bij mijn dagelijkse begeleider Stijn. Ondanks dat bleek dat het zuiveren van resazurin voor mij een te groot obstakel was om verder te gaan met katalyse. Ben je, onverminderd en met net zoveel enthousiasme, verder gegaan met mij begeleiden in mijn onderzoek. Ik heb ontzettend veel van je geleerd en ik hoop nog eens met je te kunnen samen werken als PhD!
Als tweede wil ik graag Alfons van Blaaderen bedanken voor mijn onderzoeksplek als masterstudent bij Soft Condensed Matter. Ik heb met veel plezier een jaar lang bij SCM mijn masteronderzoek gedaan.
Halverwege mijn masteronderzoek kreeg ik de kans om een nieuw project te starten in samenwerking met de TU Delft. Ik wil graag Arjan Houtepen bedanken voor deze mooie samenwerking en met name voor de uitvoerige feedback tijdens besprekingen van de resultaten. In mijn derde jaar, bij het vak Vaste Stoffen & Oppervlakken, ontmoette ik Freddy voor het eerst. Door samen met Eric naar de juiste antwoorden te vissen trokken we waarschijnlijk je aandacht aangezien je zowel mij als Eric vroeg om als duckling deel te nemen aan de synchrotron experimenten in Grenoble. Ik vind de hoeveelheid tijd die je vrijmaakt voor je studenten bewonderingswaardig en ik heb dan ook met veel plezier mijn masteronderzoek bij je gedaan.
Tijdens het voltooien van mijn masteronderzoek ben ik er achter gekomen dat ik tamelijk eenkennig ben wat betreft samenwerken. Tijdens mijn bacheloronderzoek had ik de luxepositie, zoals eerder genoemd, duckling te zijn van een team van drie PhDs: Ward, Jaco en Freddy. Uiteindelijk hebben de experimenten van dit topteam geleid tot mijn eerste bijdrage aan de wetenschap. Dat ik mijn masterthesis graag bij Freddy wilde doen is dus geen verrassing. Echter, ook Ward en Jaco hebben wederom een grote rol gespeeld tijdens mijn afstudeeronderzoek. Met Jaco heb ik, zoals eerder vermeld, experimenten mogen doen naar het elektrochemisch opladen van CdSe kwantumdeeltjes, beschreven in hoofdstuk 4. Met Ward heb ik experimenten gedaan naar hoe zoutbehandelingen de luminescentie van Perovskiet nanoplaatjes beinvloedden. Ik heb, net als tijdens mijn bachelorthesis, veel van jullie geleerd en ik hoop dat ik in de toekomst nog vaker met jullie mag samenwerken!
Elleke wil ik graag bedanken voor de prachtige CdSe/CdS deeltjes die ze gemaakt heeft voor mijn onderzoek.
Toen mijn masterscriptie al zo'n beetje ten einde liep, startte Thomas bij CMI als PhD. Ik heb het genoegen gehad om Thomas al sinds het begin van mijn studie te kennen

dus ik zou dit dankwoord minstens 2 keer zo lang kunnen maken met anekdotes over zuur/basen mengsels, zware fietstochten naar Antwerpen en lampen in de vorm van een aap. Ik zal het echter kort houden en alleen vermelden dat de dagelijkse nut square of millionaire shortcake in combinatie met een potje tafelvoetbal gezorgd hebben voor de nodige ontspanning (soms frustratie) tijdens mijn masterthesis. Verder wil ik de rest van mijn vrienden van sinds het begin van mijn scheikunde studie (genaamd de Mexers) bedanken. During my master thesis, the amount of people who worked in the student room changed considerably. I want to thank you, and all other people of SCM, for the pleasant working atmosphere during my master thesis!

Chapter 8

Appendices

8.1 Appendix A: Average number of exciton per pulse vs. laser power

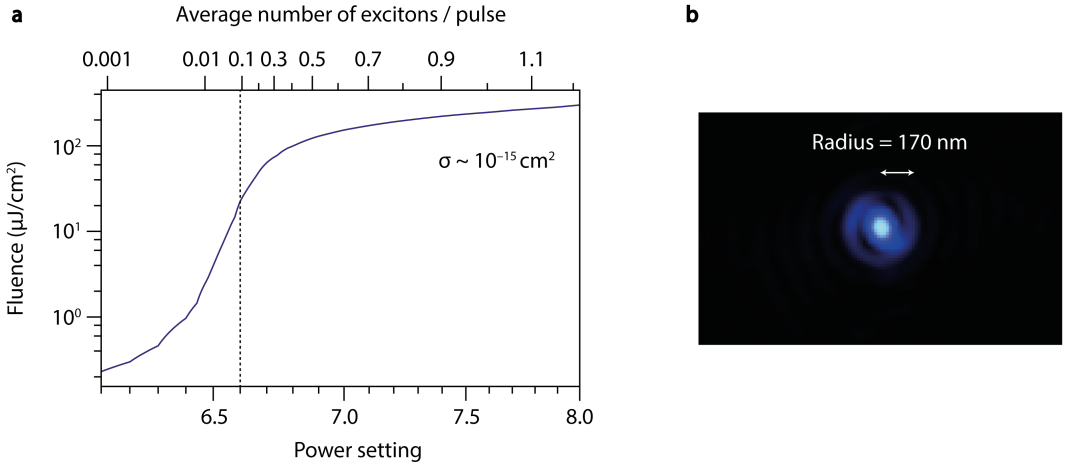

Figure 8.1: Number of excitons per pulse as function of power. (**a**) The fluence of the 405 nm laser as a function of the power setting. The laser shows a strong non-linear response of the fluence to the power setting. The dotted line shows the power setting used in all single QD experiments which amounts to an average of 0.1 excitons formed per laser pulse based on a absorption cross-section of 2×10^{-15} cm^2. (**b**) Reflection of the 405 nm laser with an aperture of 3mm before microscope input using a 520 nm dichroic mirror. Based on the magnification of $M = 100$, we determined a radius of 170 nm, which is used to determine the fluence in (**a**).

Lasers have a highly non-linear response to the power-setting of the laser driver. Therefore, to accurately determine the average number of excitons that is formed in each pulse, accurate measurements of the power are necessary . A Thorlabs S170C Optical Power Meter is used to measure the power in the laser focus at the sample stage. Figure 8.1 (**a**) shows the fluence of the 405 nm laser in the laser focus at the sample stage. The laser beam before incoupling is cut off by a 3 mm iris to avoid over-filling of the objective. The radius of the laser focus is determined by imaging the laser focus in reflection on the 520

dichroic mirror. With a magnification $M = 100$, we determine a radius of the laser focus of 170 nm. Based on this radius we determine the fluence by

$$J = \frac{PN_{\mathrm{p}}}{A_{\mathrm{laser}}}, \tag{8.1}$$

where P is the power, N_{p} is the number of pulses per second (e.g. 10^6 for 1 MHz repetition rate) and A_{laser} is the area of the laser focus. The average number of excitons formed per pulse can be determined by

$$\langle N \rangle = \frac{J\sigma}{\hbar\omega}, \tag{8.2}$$

where J is the fluence of the laser beam in J/cm^2, σ is the absorption cross section of the QD sample and $\hbar\omega$ is the energy a single photon. We assume an absorption cross section of 2×10^{-15} cm^2 based on the absorption cross section for CdSe QDs with a diameter of 3.75 nm at 405 nm obtained from Leatherdale et al.[38] We calculated the average number of exciton formed per pulse as a function of the power setting used in the single QD experiments. Figure 8.1 (**a**) shows at the upper x-axis the results, where we can see that this number changes rapidly with applied power. The dotted line at the power setting of 6.6 shows that we form approximately 0.1 excitons/pulse at a fluence of 10 μJ/cm^2. This indicates that formation of a biexciton per energy is only 1 %.

8.2 Appendix B: Hot-carrier trapping experiments

8.2.1 CdSe/CdS core/shell

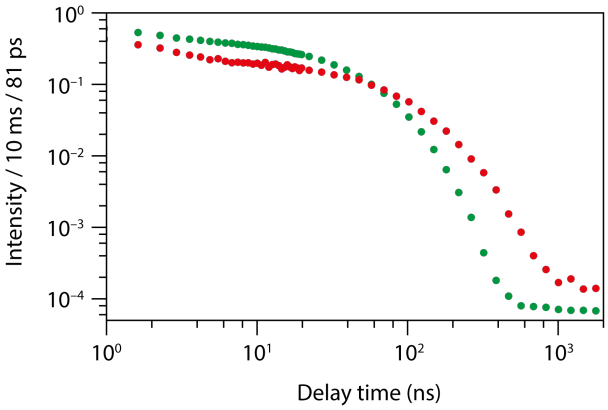

Figure 8.2: Hot carrier trapping core/shell – Measurement 1

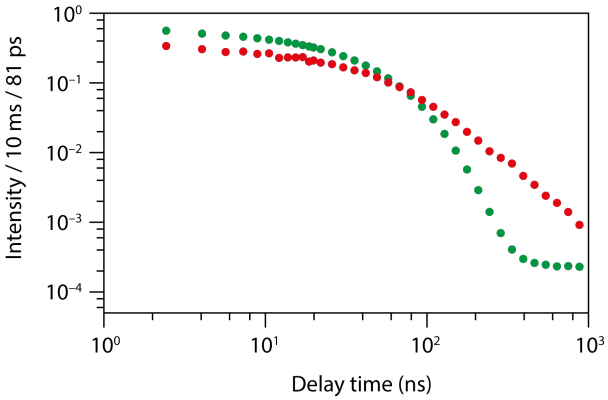

Figure 8.3: Hot carrier trapping core/shell – Measurement 2

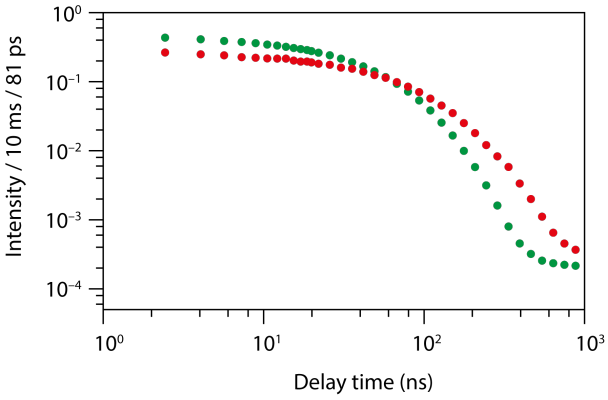

Figure 8.4: Hot carrier trapping core/shell – Measurement 3

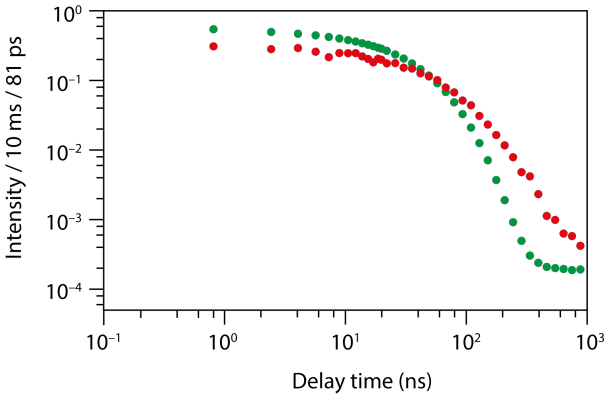

Figure 8.5: Hot carrier trapping core/shell – Measurement 4

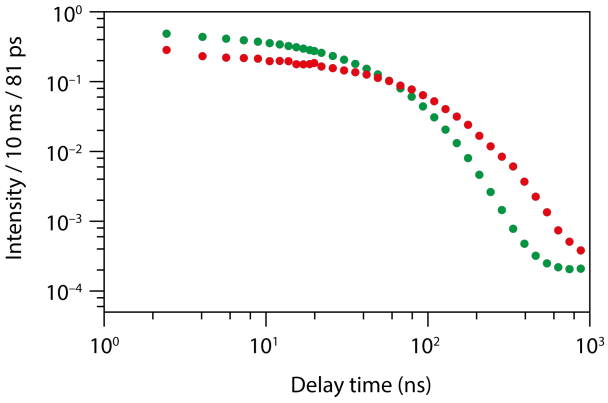

Figure 8.6: Hot carrier trapping core/shell – Measurement 5

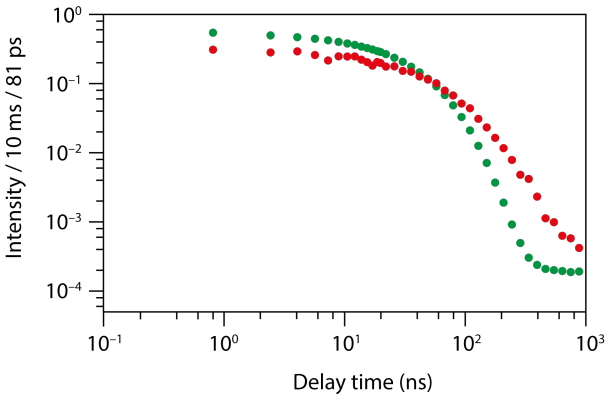

Figure 8.7: Hot carrier trapping core/shell – Measurement 6

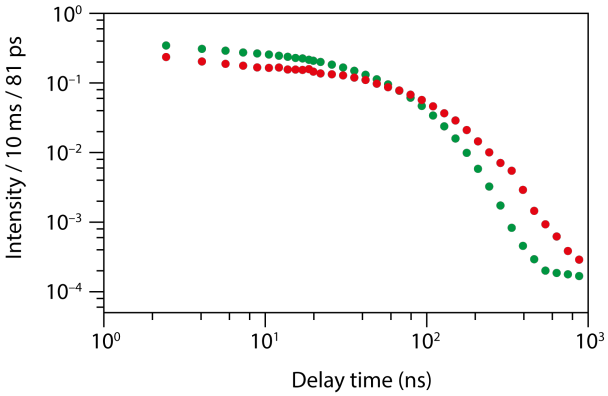

Figure 8.8: Hot carrier trapping core/shell – Measurement 7

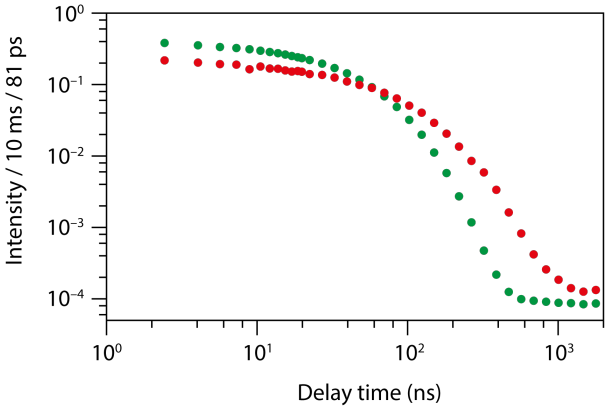

Figure 8.9: Hot carrier trapping core/shell – Measurement 8

8.2.2 CdSe core-only

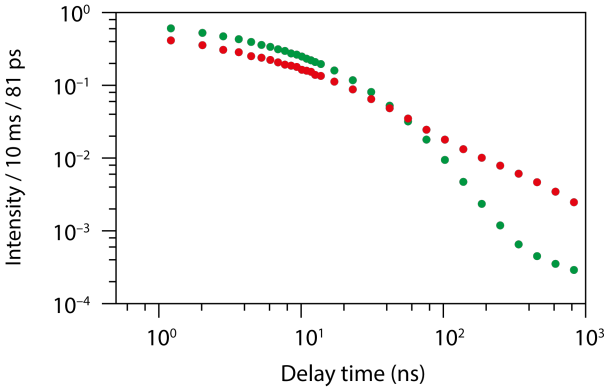

Figure 8.10: Hot carrier trapping core only – Measurement 1

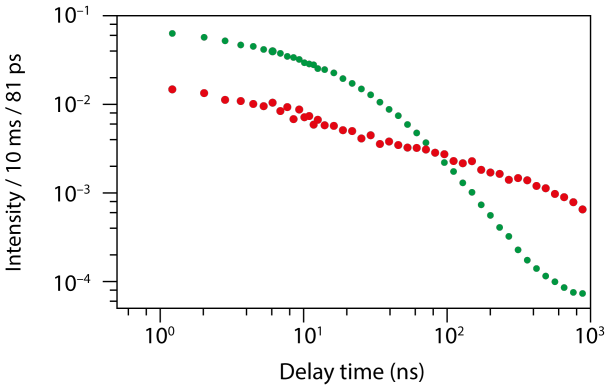

Figure 8.11: Hot carrier trapping core only – Measurement 1

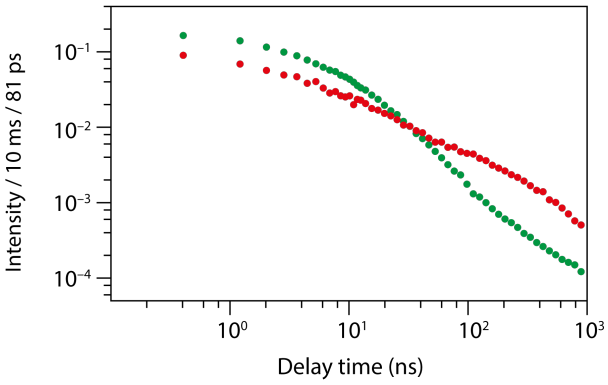

Figure 8.12: Hot carrier trapping core only – Measurement 1

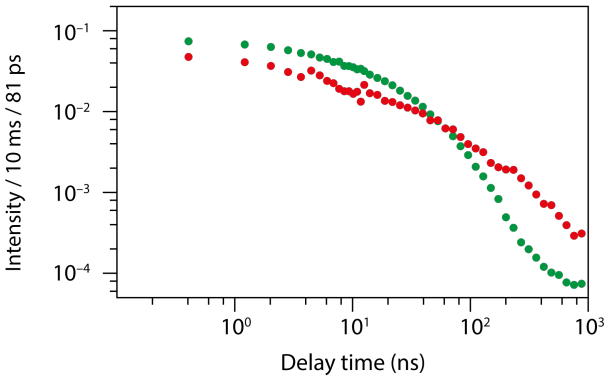

Figure 8.13: Hot carrier trapping core only – Measurement 1

8.3 Appendix C: Derivation maximum second order correlation function

The definition of the second order correlation function is given by

$$g^{(2)}(\tau) = \frac{\langle I(t)I(t+\tau)\rangle}{\langle I(t)\rangle\langle I(t+\tau)\rangle}, \tag{8.3}$$

where we have maximum correlation when the intensity at same time t is equal to the signal at $t+\tau$, e.g. $I(t) = I(t+\tau)$. We obtain for the maximum of $g^{(2)}$

$$\max[g^{(2)}(\tau)] = \frac{\langle I^2\rangle}{\langle I\rangle^2}, \tag{8.4}$$

where the expectation value of the intensity $\langle I\rangle$ and the second moment of the intensity $\langle I^2\rangle$ are given in terms of the fraction of time spent in the on or off state by

$$\begin{aligned} \langle I\rangle &= fI_{\text{on}} + (1-f)I_{\text{off}} \\ \langle I^2\rangle &= fI_{\text{on}}^2 + (1-f)I_{\text{off}}^2. \end{aligned} \tag{8.5}$$

If we plug these equation into equation 8.4, we obtain

$$\max[g^{(2)}(\tau)] = \frac{1}{\langle I\rangle^2}[I_{\text{on}}(\langle I\rangle - (1-f)I_{\text{off}}) + I_{\text{off}}(\langle I\rangle - fI_{\text{on}})] \tag{8.6}$$

which can eventually be solve to give the maximum of the second order correlation function independent of the fraction f spent in the on state

$$\max[g^{(2)}(\tau)] = \frac{I_{\text{on}} + I_{\text{off}}}{\langle I\rangle} - \frac{I_{\text{on}}I_{\text{off}}}{\langle I\rangle^2} \tag{8.7}$$

Bibliography

[1] C B Murray, D J Norris, and M G Bawendi. Synthesis and Characterization of Nearly Monodisperse CdE (E = S , Se , Te) Semiconductor Nanocrystallites. (4):8706–8715, 1993.

[2] Hendrik Utzat, Weiwei Sun, Alexander E K Kaplan, Franziska Krieg, Matthias Ginterseder, Boris Spokoyny, Nathan D Klein, Katherine E Shulenberger, Collin F Perkinson, Maksym V Kovalenko, and Moungi G Bawendi. Quantum Dots. 1072(March):1068–1072, 2019.

[3] Pascale Senellart, Glenn Solomon, and Andrew White. High-performance semiconductor quantum-dot single-photon sources. *Nature Nanotechnology*, 12(11):1026–1039, 2017.

[4] Clifton Harris and Prashant V. Kamat. Photocatalysis with CdSe nanoparticles in confined media: Mapping charge transfer events in the subpicosecond to second timescales. *ACS Nano*, 3(3):682–690, 2009.

[5] Cristian T Matea and Teodora Mocan. Quantum dots in imaging , drug delivery and sensor applications. pages 5421–5431, 2017.

[6] W W Jr and Kluwer Academic. single cadmium selenide. 383(October):802–804, 1996.

[7] M. Kuno, D. P. Fromm, H. F. Hamann, A. Gallagher, and D. J. Nesbitt. "On"/"off" fluorescence intermittency of single semiconductor quantum dots. *Journal of Chemical Physics*, 115(2):1028–1040, 2001.

[8] Al L. Efros and M. Rosen. Random telegraph signal in the photoluminescence intensity of a single quantum dot. *Physical Review Letters*, 78(6):1110–1113, 1997.

[9] Alexander L. Efros and David J. Nesbitt. Origin and control of blinking in quantum dots. *Nature Nanotechnology*, 11(8):661–671, 2016.

[10] Arianna Marchioro, Patrick J. Whitham, Kathryn E. Knowles, Troy B. Kilburn, Philip J. Reid, and Daniel R. Gamelin. Tunneling in the delayed luminescence of colloidal CdSe, Cu+-doped CdSe, and CuInS2 semiconductor nanocrystals and relationship to blinking. *Journal of Physical Chemistry C*, 120(47):27040–27049, 2016.

[11] Freddy T Rabouw, Marko Kamp, Relinde J A Van Dijk-moes, Daniel R Gamelin, A Femius Koenderink, Andries Meijerink, and Danie Vanmaekelbergh. Delayed Exciton Emission and Its Relation to Blinking in CdSe Quantum Dots. 2015.

[12] Freddy T Rabouw and Celso Mello Donega. Excited-State Dynamics in Colloidal Semiconductor. *Topics in Current Chemistry*, 374(5):1–30, 2016.

[13] Yashaswi Nandan and Mohan Singh Mehata. Wavefunction Engineering of Type-I / Type-II Excitons of CdSe / CdS Core-Shell Quantum Dots. (October 2018):1–11, 2019.

[14] A. I. Ekimov, I. A. Kudryavtsev, Al. L. Efros, T. V. Yazeva, F. Hache, M. C. Schanne-Klein, A. V. Rodina, D. Ricard, and C. Flytzanis. Absorption and intensity-dependent photoluminescence measurements on CdSe quantum dots: assignment of the first electronic transitions. *Journal of the Optical Society of America B*, 10(1):100, 1993.

[15] Celso De Mello Donega. Synthesis and properties of colloidal heteronanocrystals w. pages 1512–1546, 2011.

[16] Klaus Boldt, Nicholas Kirkwood, Gary A Beane, and Paul Mulvaney. Synthesis of Highly Luminescent and Photo-Stable, Graded Shell CdSe/Cd. pages 1–8, 2013.

[17] Kimberly H Hartstein, Christian S Erickson, Emily Y Tsui, Arianna Marchioro, and Daniel R Gamelin. Electron Stability and Negative-Tetron Luminescence in Free-Standing Colloidal n Type CdSe/CdS Quantum Dots. pages 10430–10438, 2017.

[18] Ward Van Der Stam, Solrun Gudjonsdottir, Wiel H. Evers, and Arjan J. Houtepen. Switching between Plasmonic and Fluorescent Copper Sulfide Nanocrystals. *Journal of the American Chemical Society*, 139(37):13208–13217, 2017.

[19] Christophe Galland, Yagnaseni Ghosh, Andrea Steinbrück, Milan Sykora, Jennifer A. Hollingsworth, Victor I. Klimov, and Han Htoon. Two types of luminescence blinking revealed by spectroelectrochemistry of single quantum dots. *Nature*, 479(7372):203–207, 2011.

[20] Freddy T. Rabouw, Johanna C. Van Der Bok, Piernicola Spinicelli, Benoît Mahler, Michel Nasilowski, Silvia Pedetti, Benoît Dubertret, and Daniël Vanmaekelbergh. Temporary Charge Carrier Separation Dominates the Photoluminescence Decay Dynamics of Colloidal CdSe Nanoplatelets. *Nano Letters*, 16(3):2047–2053, 2016.

[21] Kazuhiko Seki, Yoriko Sonoda, and Ryuzi Katoh. Diffusion-Mediated Delayed Fluorescence by Singlet Fission and Geminate Fusion of Correlated Triplets. *Journal of Physical Chemistry C*, 122(22):11659–11670, 2018.

[22] James K. Utterback, Amanda N. Grennell, Molly B. Wilker, Orion M. Pearce, Joel D. Eaves, and Gordana Dukovic. Observation of trapped-hole diffusion on the surfaces of CdS nanorods. *Nature Chemistry*, 8(11):1061–1066, 2016.

[23] Sidney Redner and J. R. Dorfman. *A Guide to First-Passage Processes*, volume 70. 2002.

[24] Nicholas Kirkwood, Julius O V Monchen, Ryan W Crisp, Gianluca Grimaldi, Huub A C Bergstein, Indy Fosse, Ward Van Der Stam, Ivan Infante, and Arjan J Houtepen. Finding and Fixing Traps in II VI and III V Colloidal Quantum Dots: The Importance of Z Type Ligand Passivation. 2018.

[25] Gregory Kalyuzhny and Royce W. Murray. Ligand effects on optical properties of CdSe nanocrystals. *Journal of Physical Chemistry B*, 109(15):7012–7021, 2005.

[26] David R Baker and Prashant V Kamat. Tuning the Emission of CdSe Quantum Dots by Controlled Trap Enhancement. 26(21):11272–11276, 2010.

[27] Arianna Cretí, Marco Anni, Margherita Zavelani Rossi, Guglielmo Lanzani, Gabriella Leo, Fabio Della Sala, Liberato Manna, and Mauro Lomascolo. Ultrafast carrier dynamics in core and core/shell CdSe quantum rods: Role of the surface and interface defects. *Physical Review B - Condensed Matter and Materials Physics*, 72(12):1–10, 2005.

[28] Luigi Carbone, Concetta Nobile, Milena De Giorgi, Fabio Della Sala, Giovanni Morello, Pierpaolo Pompa, Martin Hytch, Etienne Snoeck, Angela Fiore, Isabella R Franchini, Monica Nadasan, Albert F Silvestre, Letizia Chiodo, Stefan Kudera, Roberto Cingolani, Roman Krahne, and V Arnesano. Synthesis and Micrometer-Scale Assembly of Colloidal CdSe / CdS Nanorods Prepared by a Seeded Growth Approach. 2007.

[29] W. William Yu, Lianhua Qu, Wenzhuo Guo, and Xiaogang Peng. Erratum: Experimental Determination of the Extinction Coefficient of CdTe, CdSe and CdS Nanocrystals (Chemistry of Materials (2003) 15, 14 (2854-2860)). *Chemistry of Materials*, 16(3):560, 2004.

[30] Urte Hotje, Christoph Rose, and Michael Binnewies. Lattice constants and molar volume in the system ZnS, ZnSe, CdS, CdSe. *Solid State Sciences*, 5(9):1259–1262, 2003.

[31] Dainis Dravins, Daniel Faria, and Bo Nilsson. Avalanche diodes as photon-counting detectors in astronomical photometry. *Optical and IR Telescope Instrumentation and Detectors*, 4008(August 2000):298, 2003.

[32] Abdul Waris Ziarkash, Siddarth Koduru Joshi, Mario Stipčević, and Rupert Ursin. Comparative study of afterpulsing behavior and models in single photon counting avalanche photo diode detectors. *Scientific Reports*, 8(1):1–8, 2018.

[33] Picoquant. PDM Series specifics. Technical report.

[34] Ou Chen, Jing Zhao, Vikash P Chauhan, Jian Cui, Cliff Wong, Daniel K Harris, He Wei, Hee-sun Han, Dai Fukumura, Rakesh K Jain, and Moungi G Bawendi. linewidths and suppressed blinking. *Nature Materials*, 12(5):445–451, 2013.

[35] Gangcheng Yuan, Daniel E. Gómez, Nicholas Kirkwood, Klaus Boldt, and Paul Mulvaney. Two Mechanisms Determine Quantum Dot Blinking. *ACS Nano*, 12(4):3397–3405, 2018.

[36] Freddy T. Rabouw, Roman Vaxenburg, Artem A. Bakulin, Relinde J.A. Van Dijk-Moes, Huib J. Bakker, Anna Rodina, Efrat Lifshitz, Alexander L. Efros, A. Femius Koenderink, and Daniël Vanmaekelbergh. Dynamics of Intraband and Interband Auger Processes in Colloidal Core-Shell Quantum Dots. *ACS Nano*, 9(10):10366–10376, 2015.

[37] Heinz Gerischer and Walter Ekardt. Fermi levels in electrolytes and the absolute scale of redox potentials. *Applied Physics Letters*, 43(4):393–395, 1983.

[38] C A Leatherdale, F V Mikulec, and M G Bawendi. On the Absorption Cross Section of CdSe Nanocrystal Quantum Dots. 02139:7619–7622, 2002.